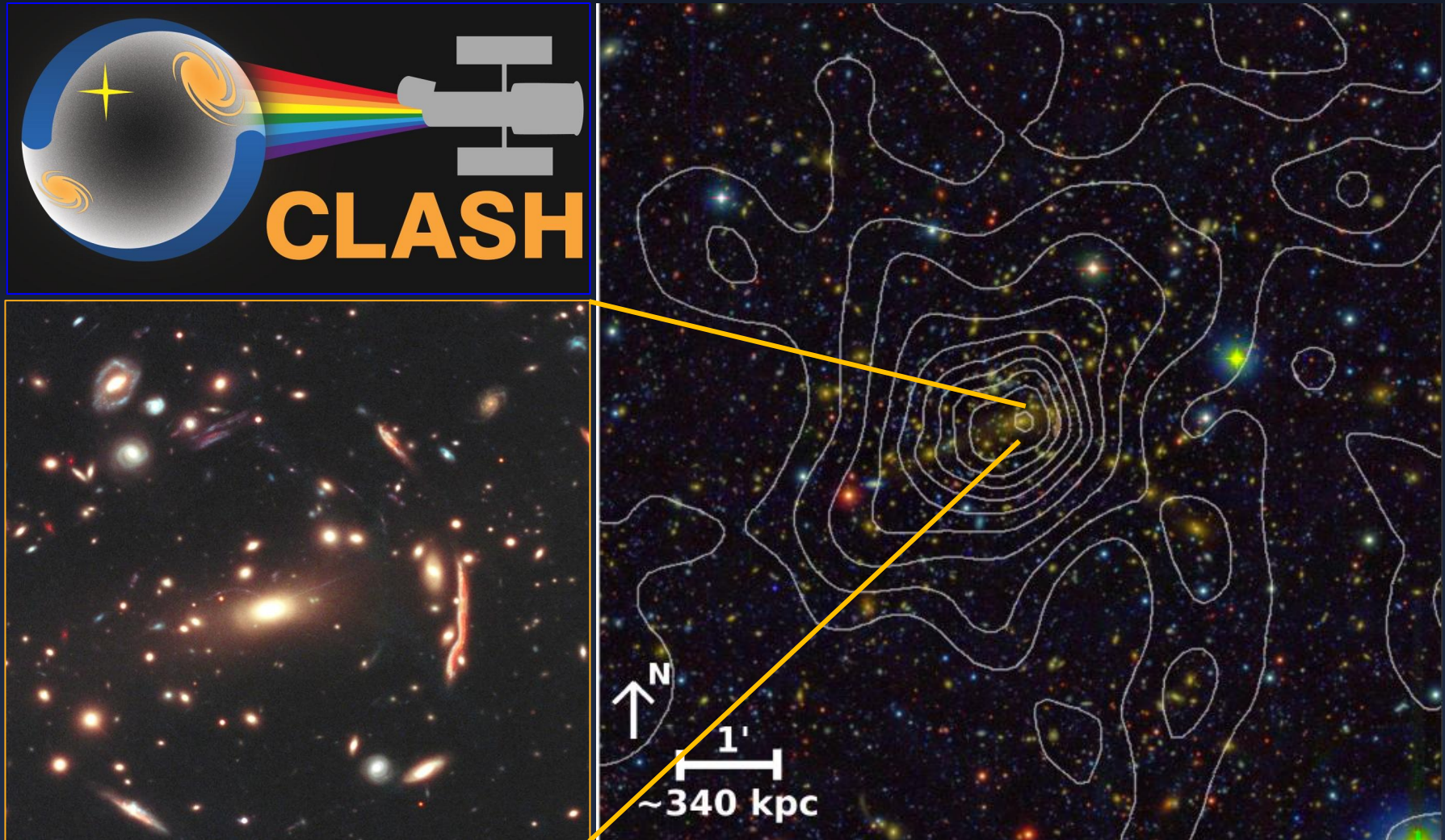


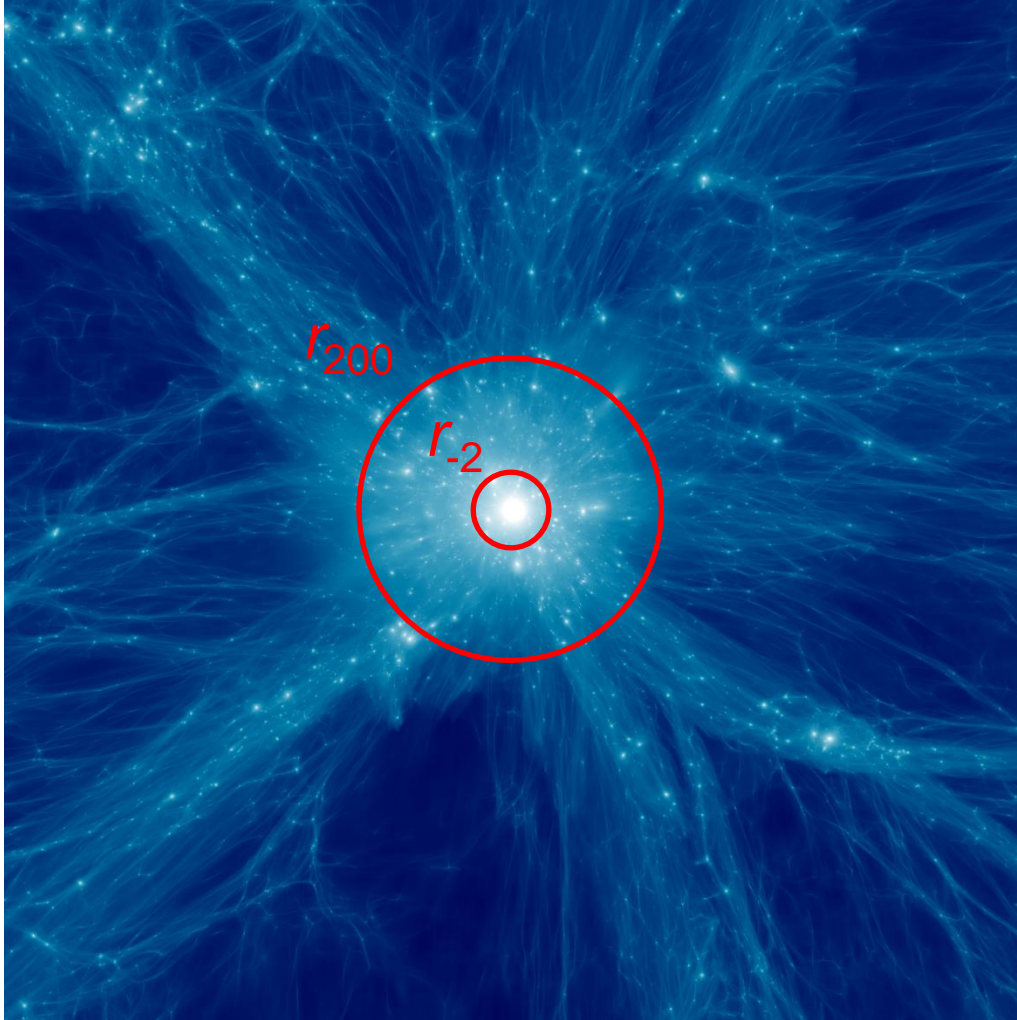
The Full Strength of Cluster Gravitational Lensing: *Mass Distribution of Galaxy Clusters from the CLASH Survey*

Cluster **L**ensing **A**nd **S**upernova survey with **H**ubble



Keiichi Umetsu (ASIAA, Taiwan)

Cluster Gravitational Lensing



Diemer & Mansfield

Key Objectives

Intra-halo structure (1h)

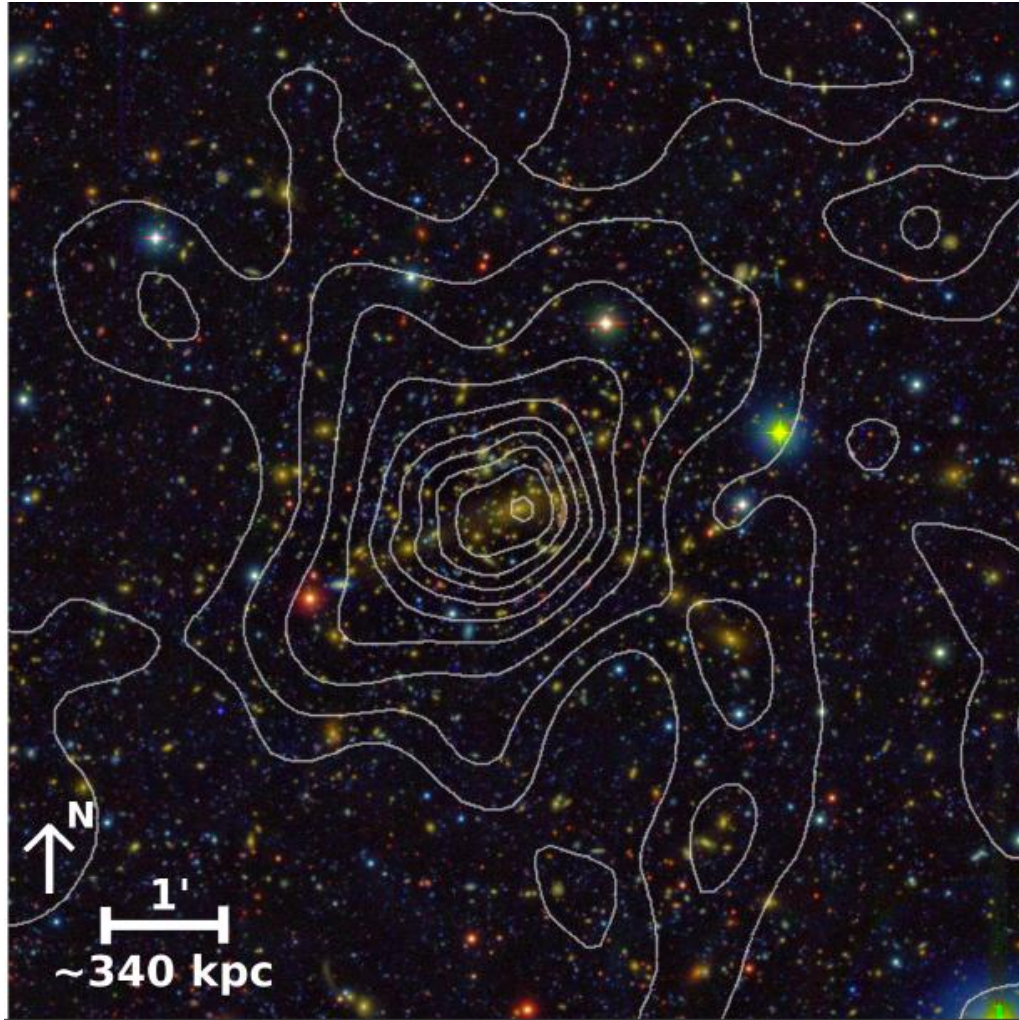
- Halo density profile, $\rho(r)$
- Halo mass, M_{Δ}
- Concentration, $c = r_{200}/r_{-2}$
- Shape parameter, α_E

$$\frac{d \ln \rho(r)}{d \ln r} = -2 \left(\frac{r}{r_{-2}} \right)^{\alpha_E}$$

Surrounding LSS (2h)

- Halo bias $b_h(M, z)$
- Assembly bias
- Clustering strength σ_8

Cluster Gravitational Lensing



Key Objectives

Intra-halo structure (1h)

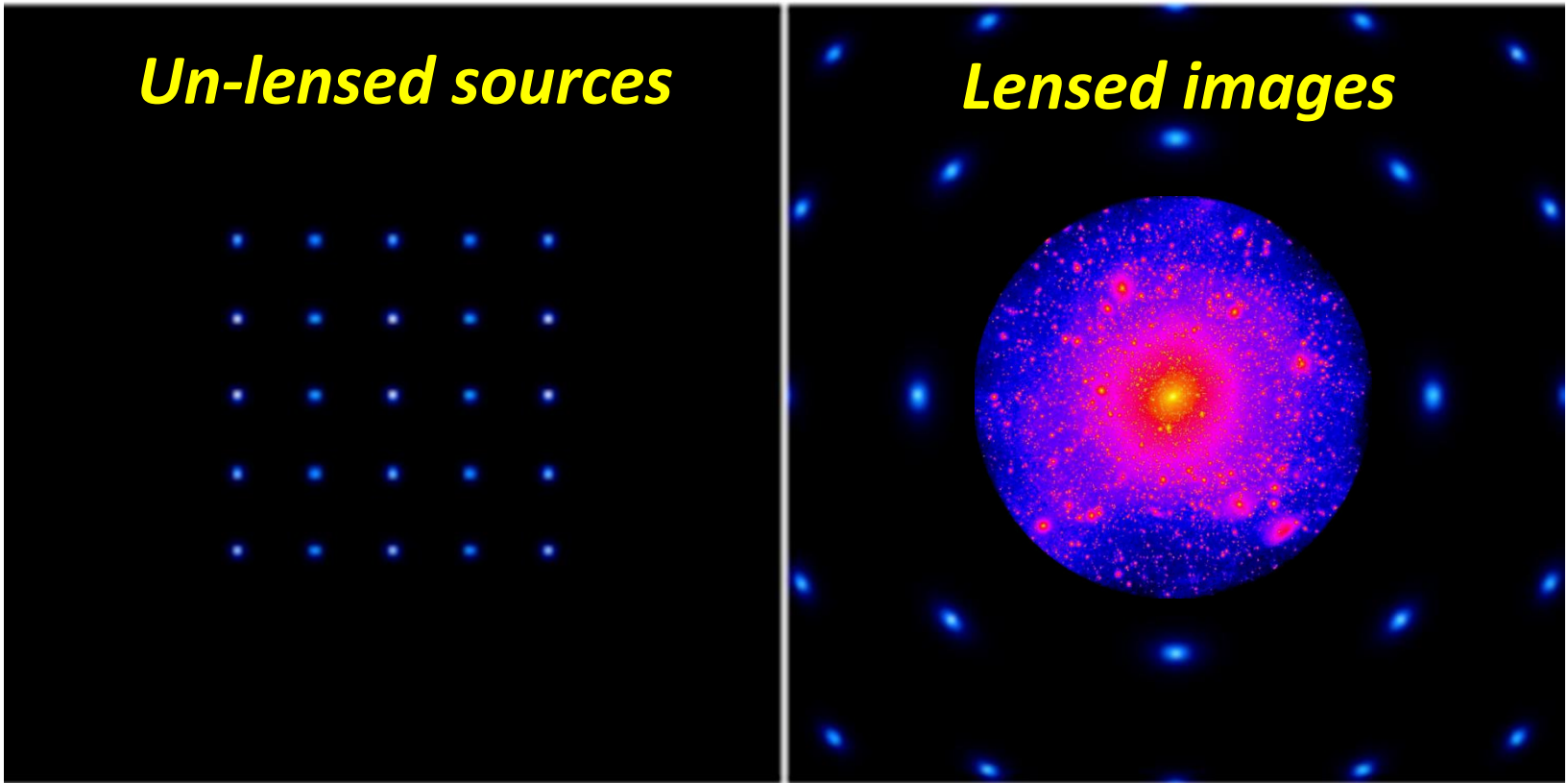
- Halo density profile, $\rho(r)$
- Halo mass, M_{Δ}
- Concentration, $c = r_{200}/r_{-2}$
- Shape parameter, α_E

$$\frac{d \ln \rho(r)}{d \ln r} = -2 \left(\frac{r}{r_{-2}} \right)^{\alpha_E}$$

Surrounding LSS (2h)

- Halo bias $b_h(M, z)$
- Assembly bias
- Clustering strength σ_8

Weak Lensing Shear and Magnification



Un-lensed sources

Lensed images

- **Shear**

Sensitive to “modulated” matter density

✓ Shape distortion: $\delta e_+ \sim \gamma_+$

$$\Sigma_c \gamma_+ = \Delta \Sigma(R) \equiv \Sigma(< R) - \Sigma(R)$$

- **Magnification**

Sensitive to “total” matter density

✓ Flux amplification: μF

✓ Area distortion: $\mu \Delta \Omega$

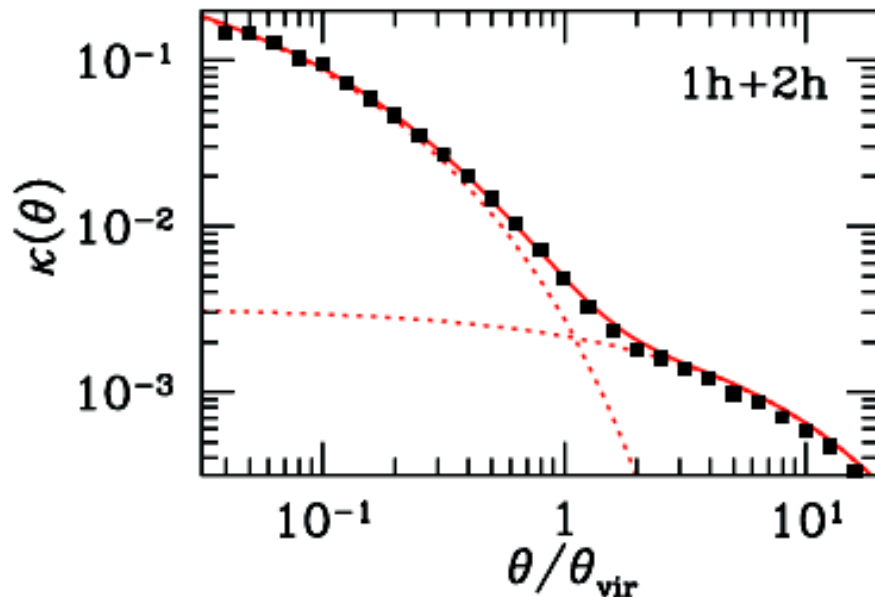
$$\mu \approx 1 + 2\kappa; \quad \Sigma_c \kappa = \Sigma(R)$$

Shear doesn't see mass sheet

Averaged lensing profiles in/around LCDM halos (Oguri & Hamana 11)

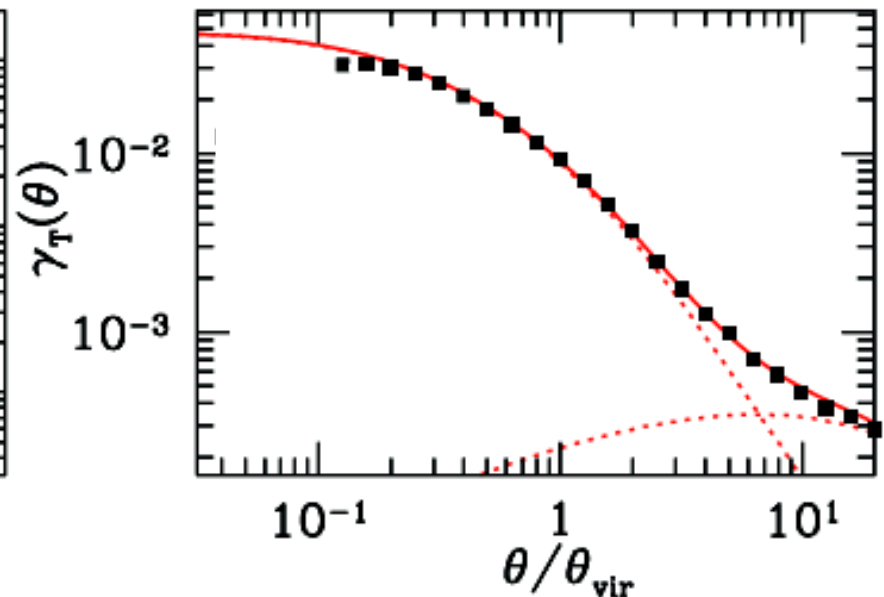
Total

$$\kappa = \Sigma(R) / \Sigma_c$$



Modulated

$$\gamma_+ = \Delta\Sigma(R) / \Sigma_c$$



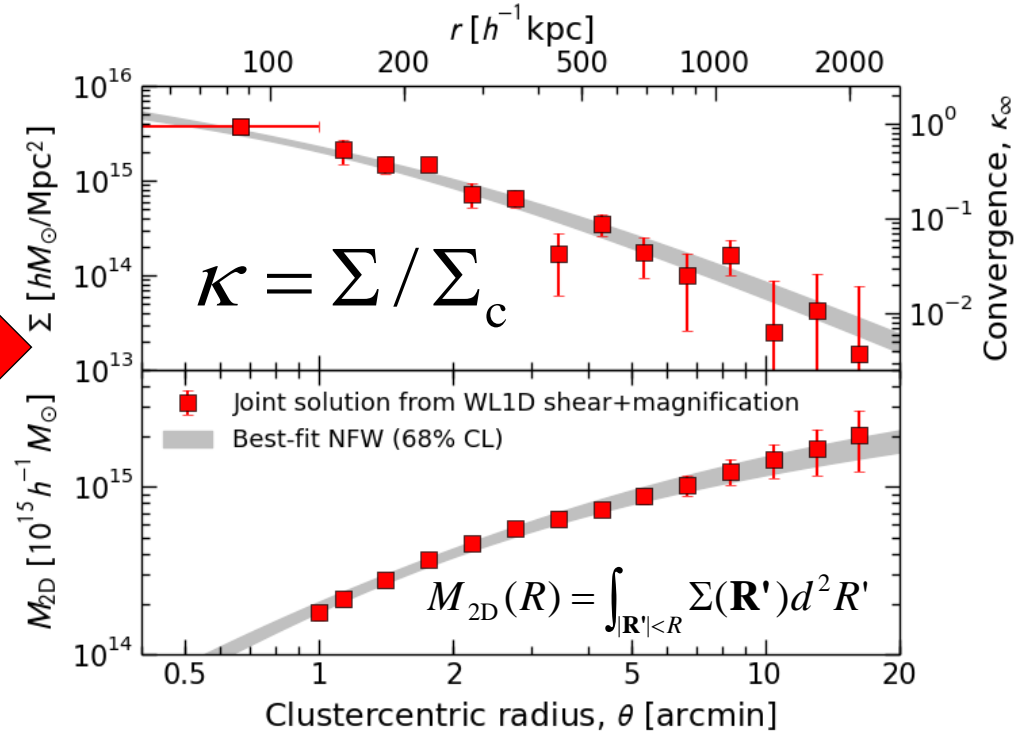
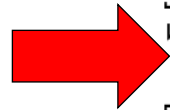
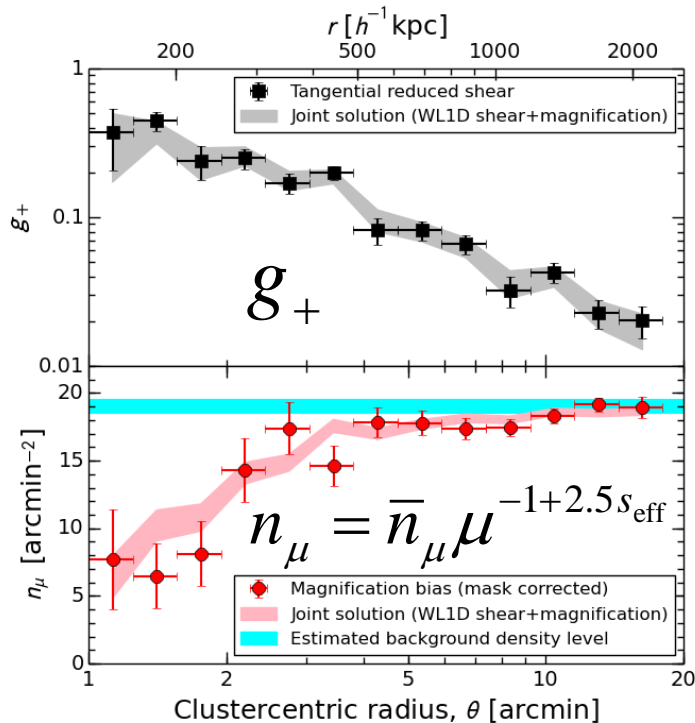
- Tangential shear is a powerful probe of **1-halo term**, or **intra-halo structure**.
- Shear alone cannot recover absolute mass, known as **mass-sheet degeneracy**:

γ remains unchanged by $\kappa \rightarrow \kappa + \text{const.}$

Combining Weak-Lensing Shear and Magnification

$$p(\boldsymbol{\kappa} \mid \text{WL}) \propto p(\text{WL} \mid \boldsymbol{\kappa}) p(\boldsymbol{\kappa}) = p(\mathbf{g}_+ \mid \boldsymbol{\kappa}) p(\mathbf{n}_\mu \mid \boldsymbol{\kappa}) p(\boldsymbol{\kappa})$$

Subaru/Suprime-Cam data (e.g., Umetsu+11a,15a)



- Mass-sheet degeneracy broken
- Total statistical precision improved by $\sim 20\text{-}30\%$
- Calibration uncertainties marginalized over: $c = \{\langle W \rangle_s, f_{W,s}, \langle W \rangle_\mu, \bar{n}_\mu, s_{\text{eff}}\}$.

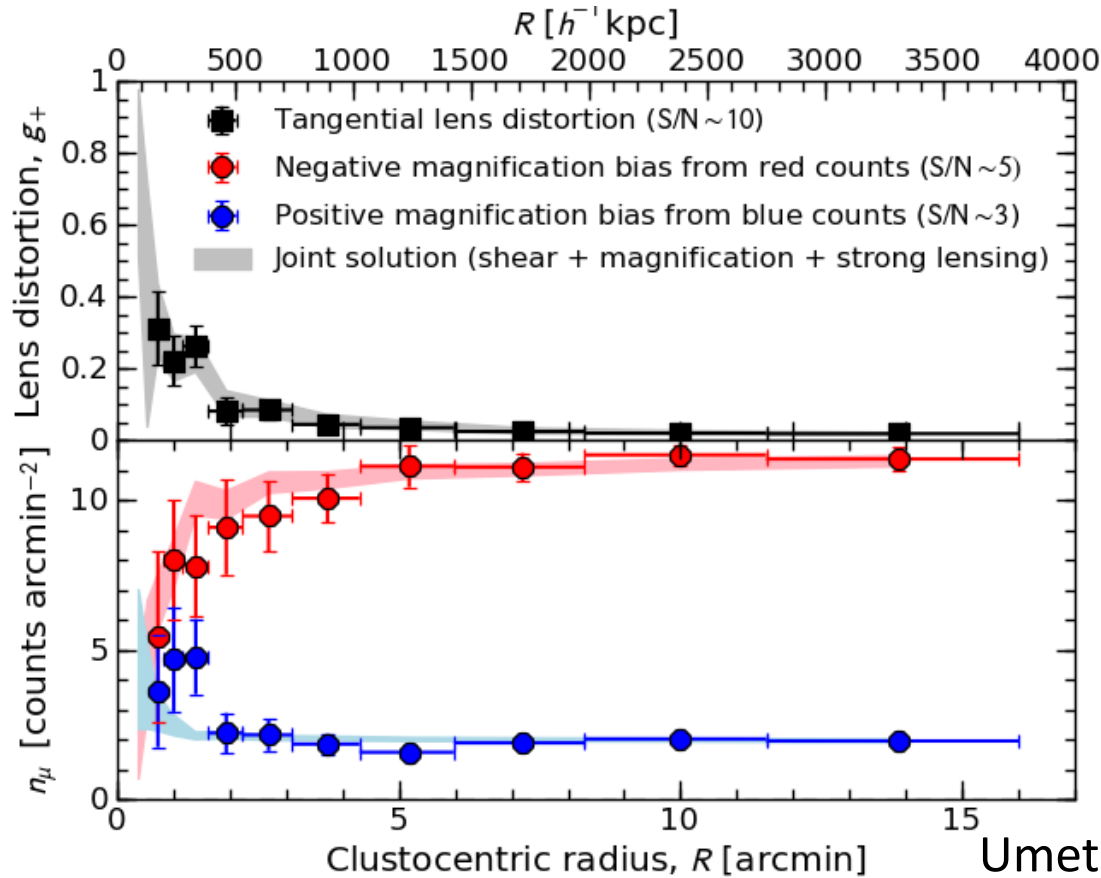
Multi-probe Lensing Approach

Combining azimuthally-averaged strong and weak lensing observables

$$\{M_{2D,i}\}_{i=1}^{N_{SL}}, \{\langle g_{+,i} \rangle\}_{i=1}^{N_{WL}}, \{\langle n_{\mu,i} \rangle\}_{i=1}^{N_{WL}}.$$

$$M_{2D}(R) = \int_{|\mathbf{R}'| < R} \Sigma(\mathbf{R}') d^2 R'$$

$$p(\boldsymbol{\kappa} | \text{WL}, \text{SL}) \propto p(\text{WL}, \text{SL} | \boldsymbol{\kappa}) p(\boldsymbol{\kappa}) = p(\mathbf{g}_+ | \boldsymbol{\kappa}) p(\mathbf{n}_\mu | \boldsymbol{\kappa}) p(\mathbf{M}_{2D} | \boldsymbol{\kappa}) p(\boldsymbol{\kappa})$$



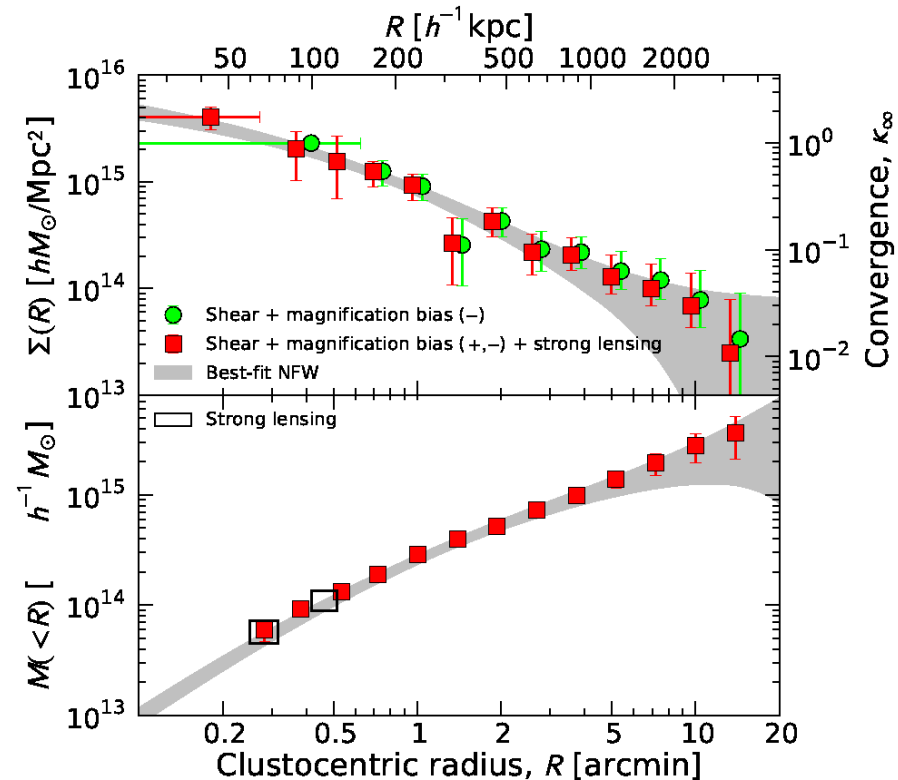
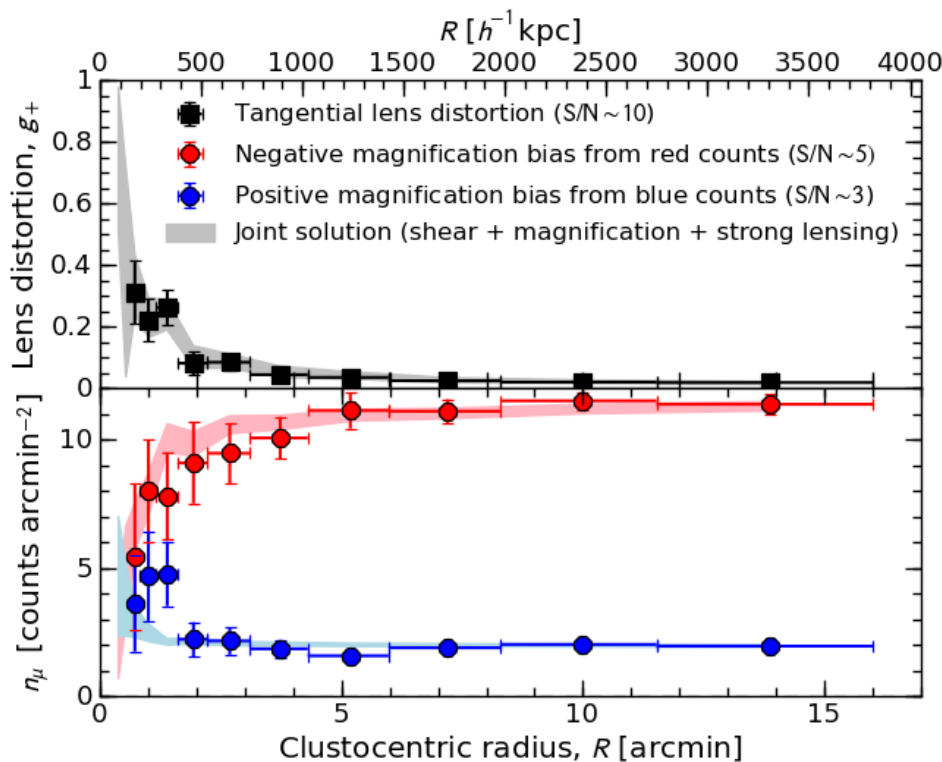
Multi-probe Lensing Approach

Combining azimuthally-averaged strong and weak lensing observables

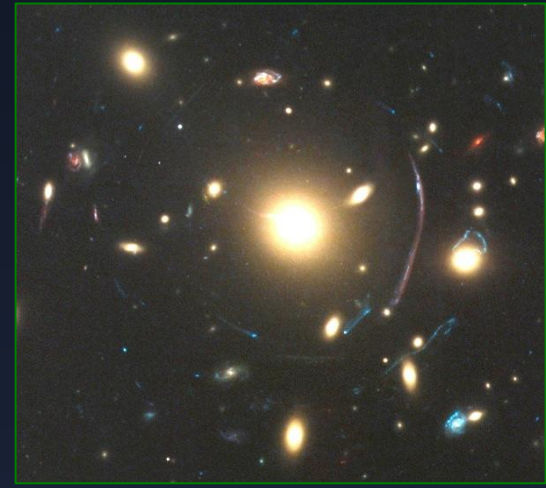
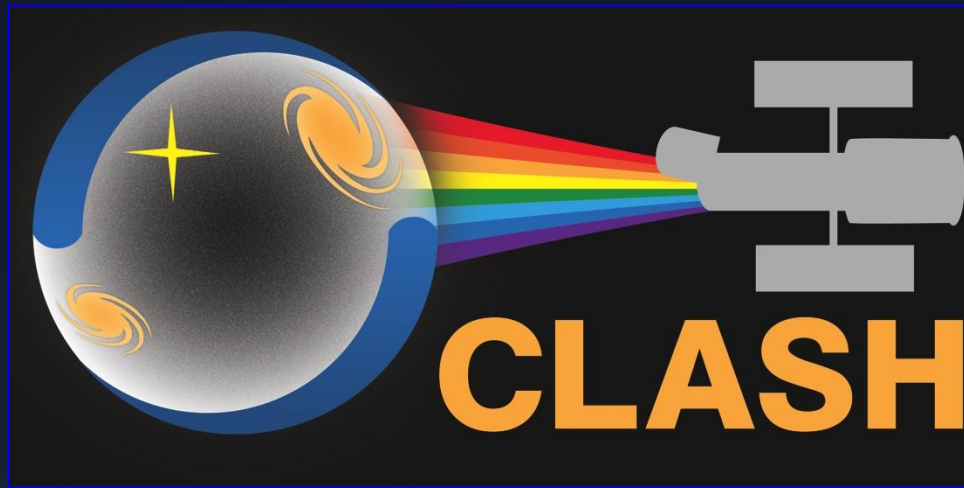
$$\{M_{2D,i}\}_{i=1}^{N_{SL}}, \{\langle g_{+,i} \rangle\}_{i=1}^{N_{WL}}, \{\langle n_{\mu,i} \rangle\}_{i=1}^{N_{WL}}.$$

$$M_{2D}(R) = \int_{|\mathbf{R}'| < R} \Sigma(\mathbf{R}') d^2 R'$$

$$p(\boldsymbol{\kappa} | \text{WL}, \text{SL}) \propto p(\text{WL}, \text{SL} | \boldsymbol{\kappa}) p(\boldsymbol{\kappa}) = p(\mathbf{g}_+ | \boldsymbol{\kappa}) p(\mathbf{n}_\mu | \boldsymbol{\kappa}) p(M_{2D} | \boldsymbol{\kappa}) p(\boldsymbol{\kappa})$$



Cluster Lensing And Supernova survey with Hubble

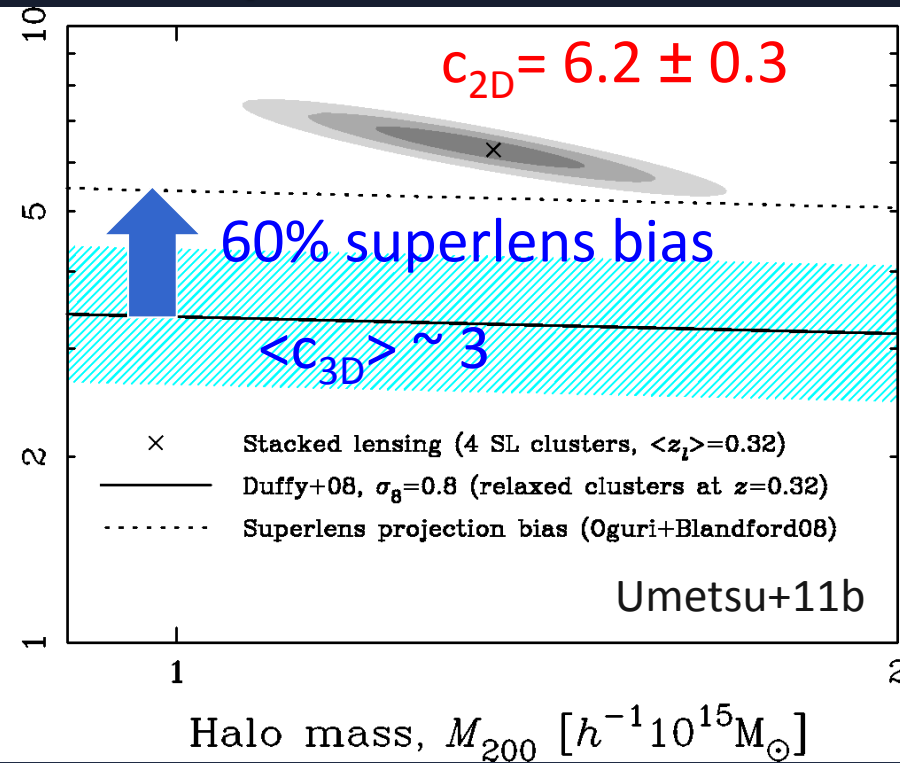
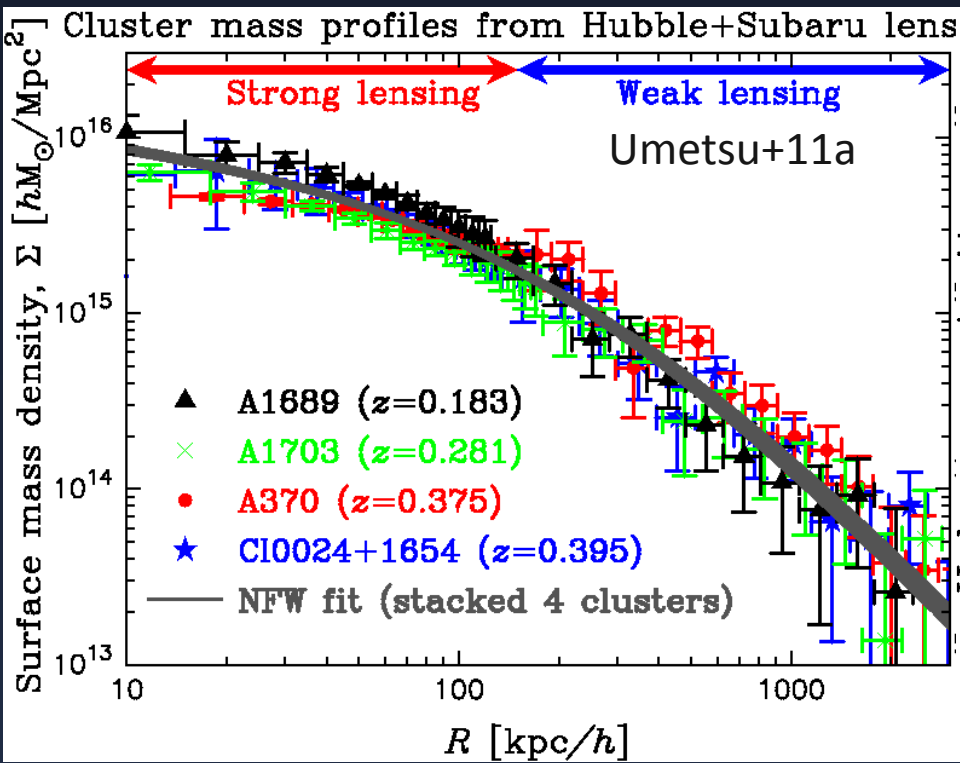


PI. Marc Postman (STScI)

<http://www.stsci.edu/~postman/CLASH/Home.html>

CLASH Objectives & Motivation

Before CLASH (2010), deep-multicolor Strong (*HST*) + Weak (*Subaru*) lensing data only available for a handful of “super lens” clusters

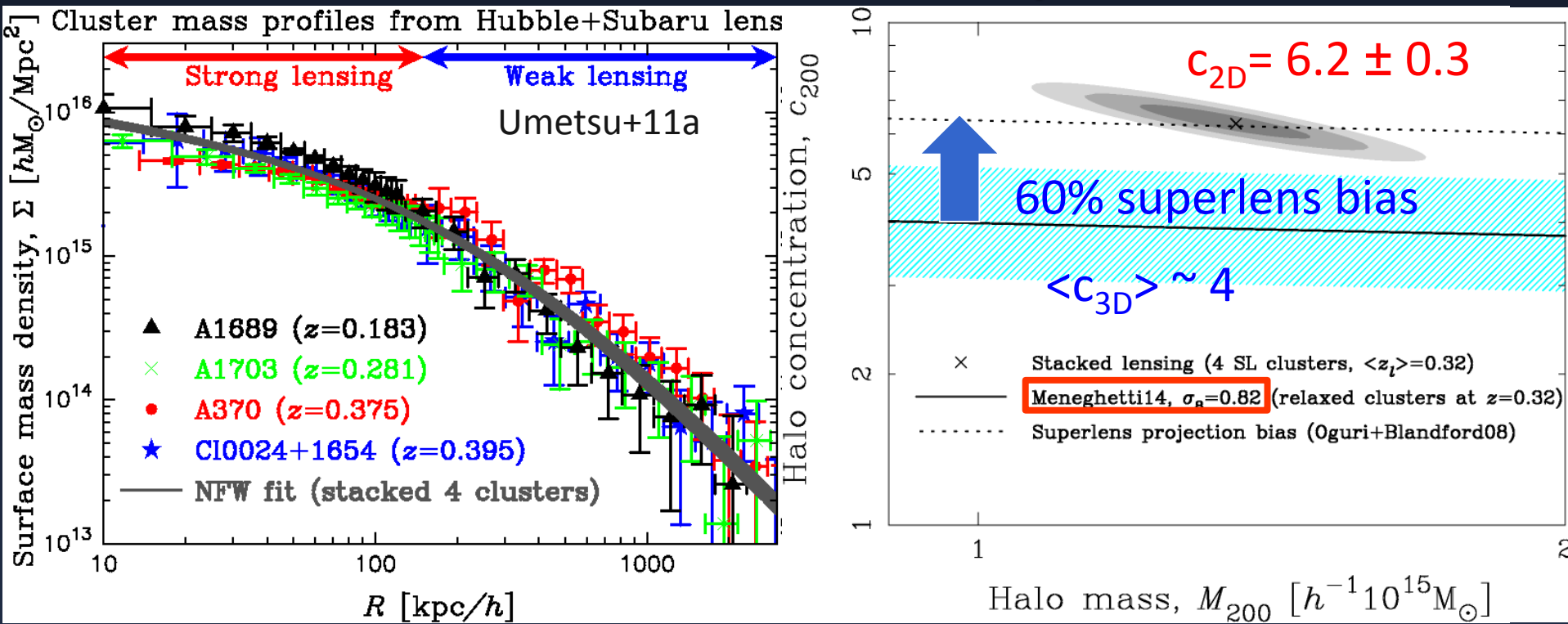


Total mass profile shape: consistent w self-similar NFW (cf. Newman+13; Okabe+13)

Degree of concentration: predicted superlens correction not enough if $\langle c_{\text{LCDM}} \rangle \sim 3$?

CLASH Objectives & Motivation

Before CLASH (2010), deep-multicolor Strong (*HST*) + Weak (*Subaru*) lensing data only available for a handful of “super lens” clusters



Total mass profile shape: consistent w self-similar NFW (cf. Newman+13; Okabe+13)

Degree of concentration: predicted superlens correction is just enough if $\langle c_{\text{LCDM}} \rangle \sim 4$



CLASH X-ray-selected Subsample

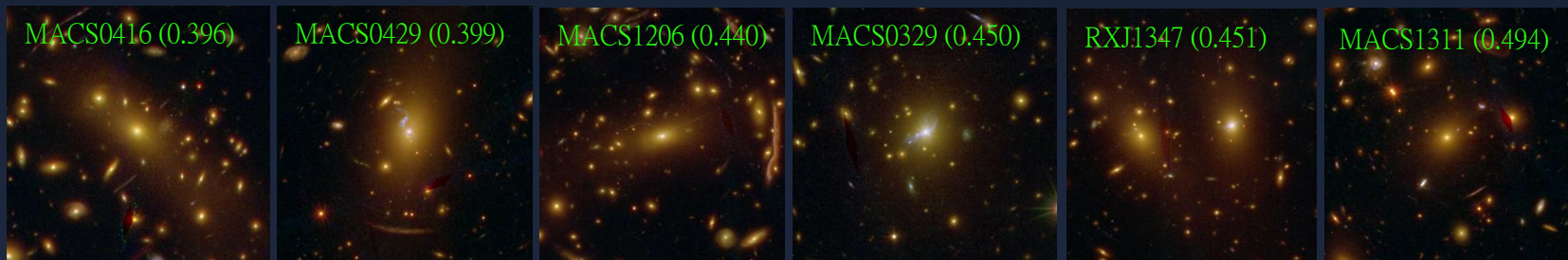
- **High-mass clusters with smooth X-ray morphology**
 - $T_x > 5\text{keV}$ ($M_{200c} > 5e14M_{\text{sun}}/h$)
 - Small BCG to X-ray-peak offset, $\sigma_{\text{off}} \sim 10\text{kpc}/h$
 - Smooth regular X-ray morphology
 - **Optimized for radial-profile analysis**
- **CLASH theoretical predictions** (Meneghetti+14)
 - Composite relaxed (70%) and unrelaxed (30%) clusters
 - Mean $\langle c_{200c} \rangle = 3.9$, $c_{200c} = [3, 6]$
 - Small scatter in c_{200c} : $\sigma(\ln c_{200c}) = 0.16$
 - Largely free of orientation bias ($\sim 2\%$ in $\langle M_{3D} \rangle$)
 - $>90\%$ of CLASH clusters to have strong-lensing features



**CLASH: Joint Analysis of Strong-lensing,
Weak-lensing Shear and Magnification
Data
for 20 CLASH Galaxy Clusters**

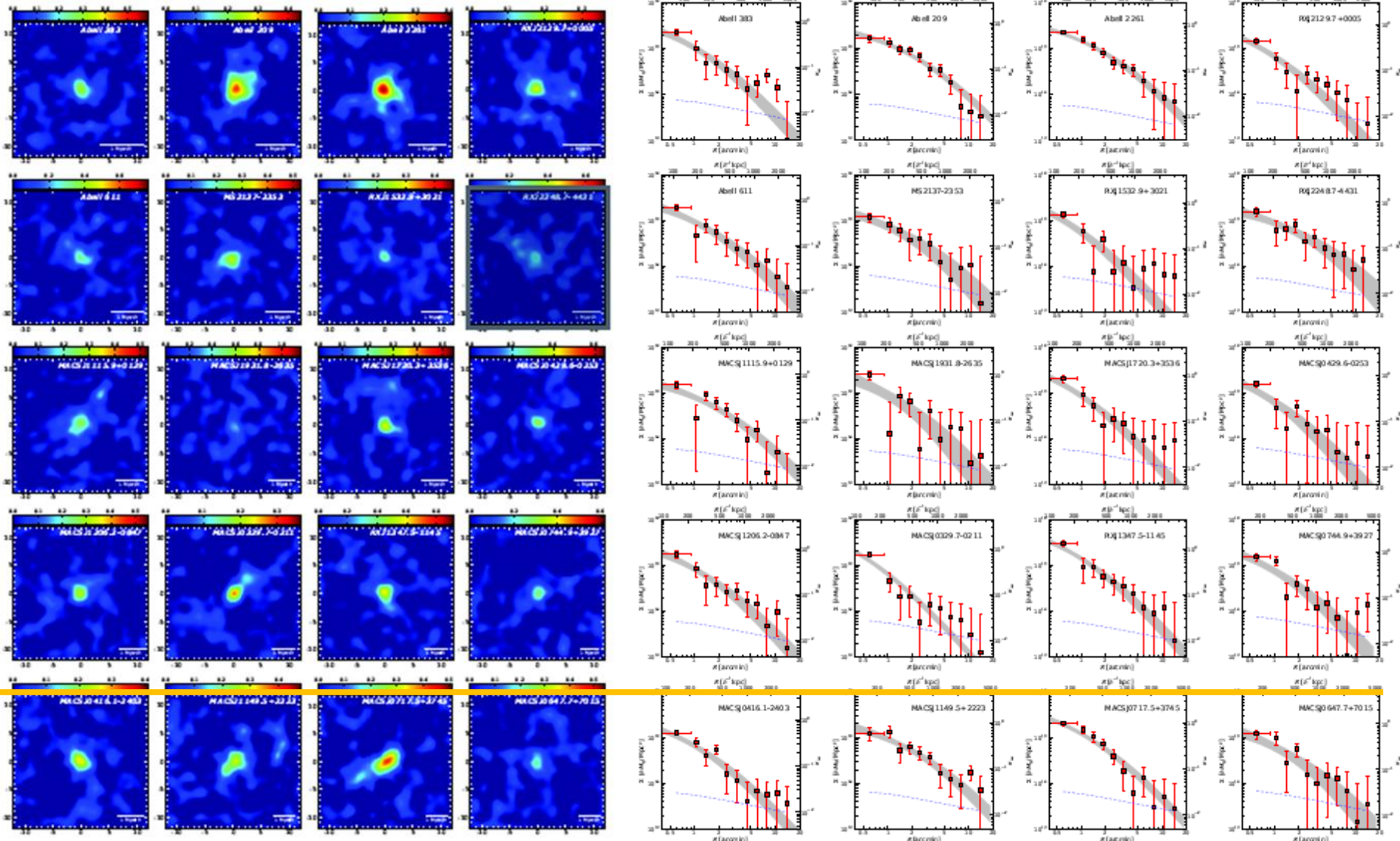
Umetsu et al. 2015b, arXiv:1507.04385
(submitted to ApJ in mid July)

CLASH *HST* Lensing Dataset





CLASH *Subaru* Weak-lensing Dataset

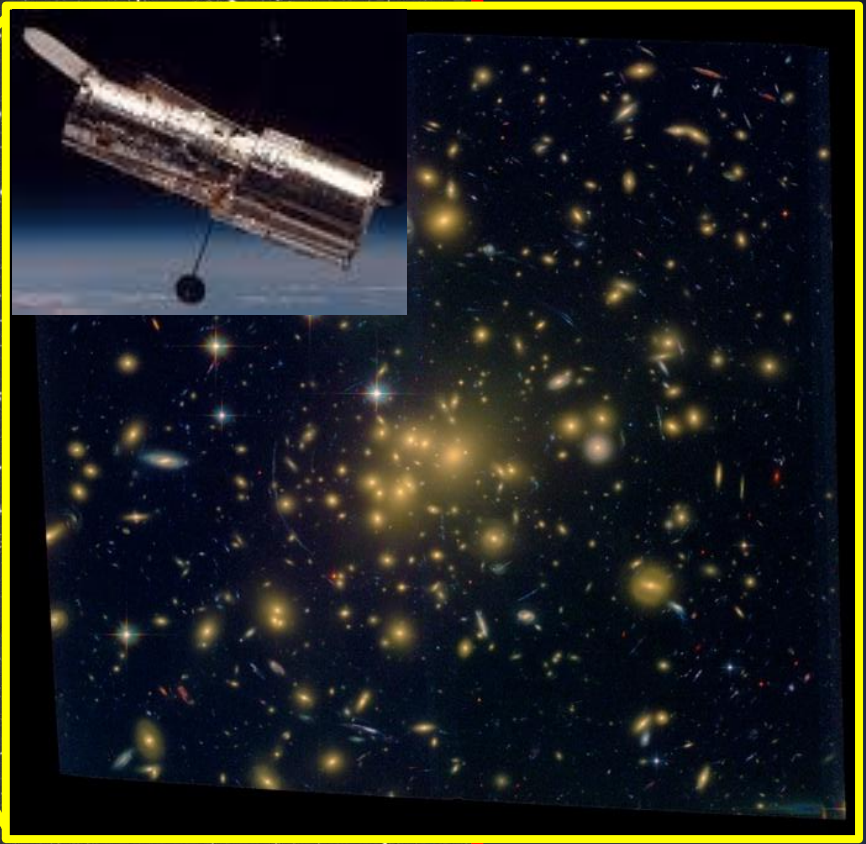


No WL data for M1311, M2129

Umetsu, Medezinski, Nonino et al. 2014, *ApJ*, 795, 163

Subaru/Suprime-Cam multi-color imaging for wide-field

High-resolution space imaging with *HST* (ACS/WFC3) for strong lensing



34 arcmin



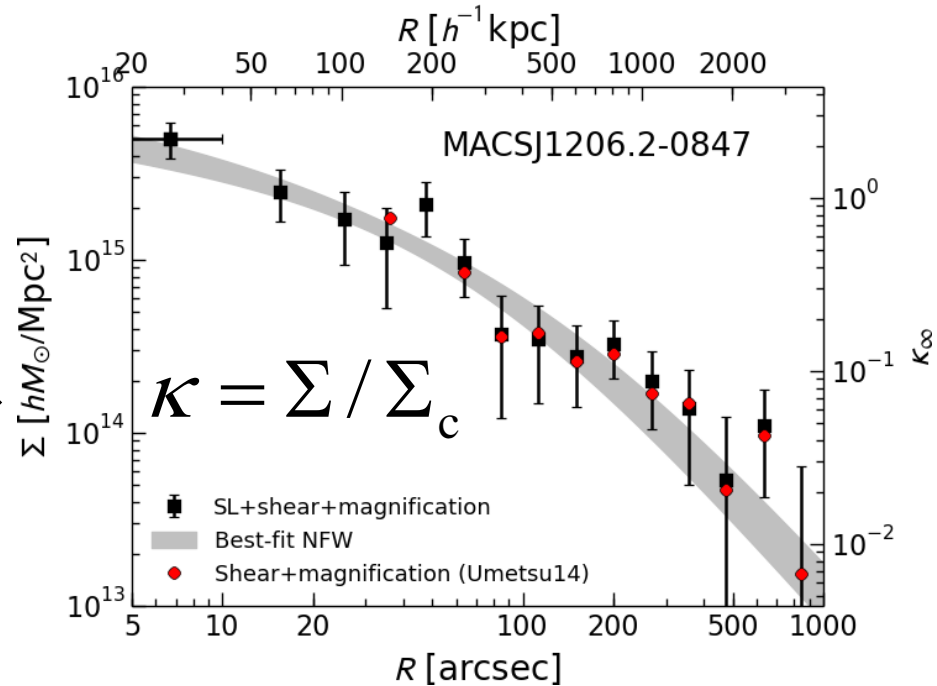
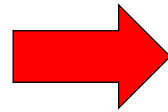
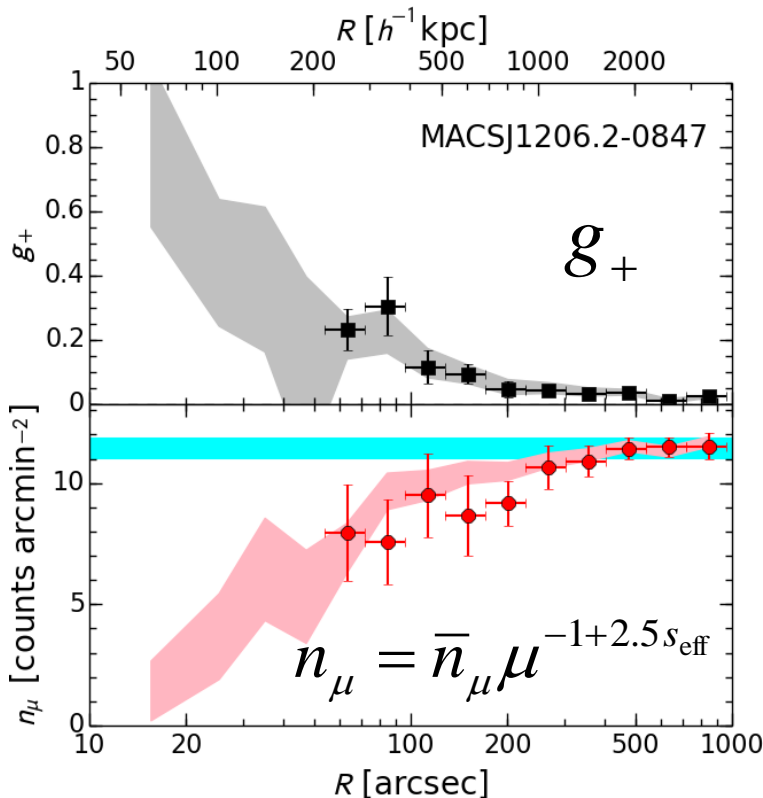
Joint Analysis of Strong-lensing, Weak-lensing Shear and Magnification Constraints

$$\{M_{2D,i}\}_{i=1}^{N_{SL}}, \{\langle g_{+,i} \rangle\}_{i=1}^{N_{WL}}, \{\langle n_{\mu,i} \rangle\}_{i=1}^{N_{WL}}.$$

HST multiple-image constraints on $M_{2D}(<R)$ (Zitrin et al. 15, *ApJ*, 801, 44)

$$\Delta = 10'' (R_{Ein}/22'')^{1/2} (N/17)^{-1/2} \text{ sampling, } R_{max} \sim 2 \langle R_{Ein} \rangle \sim 40''$$

Strong-lensing mass integration radii: $R=(10'', 20'', 30'', 40'')$



$\langle \chi^2/dof \rangle = 0.95$ for 20 CLASH clusters

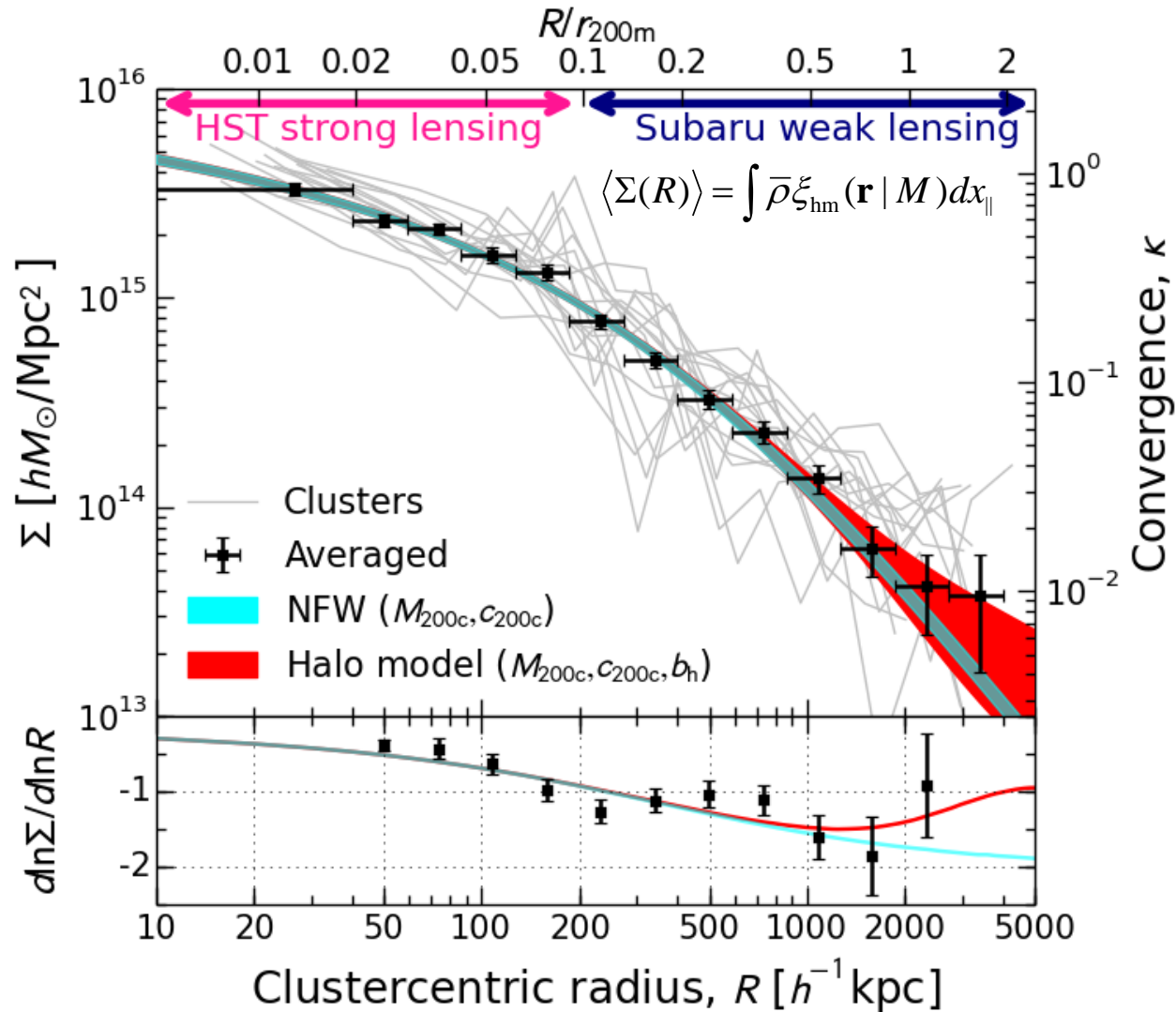


CLASH Stacked Full-lensing Analysis of the X-ray-selected Subsample

Umetsu et al. 2015b, arXiv:1507.04385



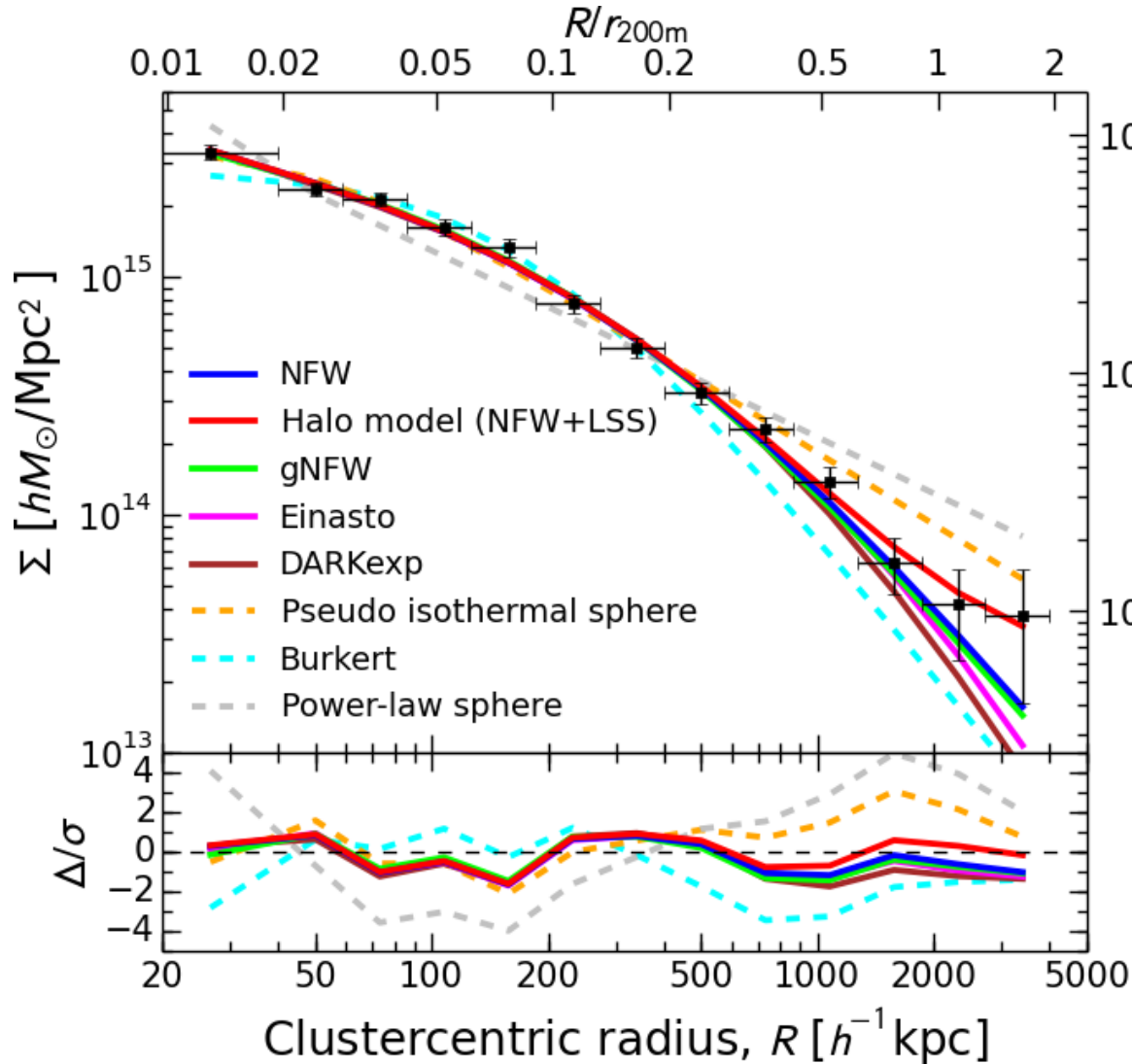
Ensemble-averaged Surface Mass Density Profile



33 σ detection of the ensemble-averaged mass profile out to $\sim 2r_{200m}$



Characterizing the Averaged Mass Profile Shape



$$\Sigma(R) = \int dl \Delta\rho(r),$$

Convergence, κ

Models:

- 1. No 2-halo term, no truncation**
($f_t=1, \rho_{2h}=0$)
- 2. With 2-halo term (Tinker+10)**

$$\Delta\rho(r) = f_t(r) \rho_h(r) + \rho_{2h}(r),$$

$$f_t(r) = \left[1 + \left(\frac{r}{r_t} \right)^2 \right]^{-2},$$



Comparison of Best-fit Models

Acceptable fits: p values (PTE) > 0.05

Table 4
Best-fit models for the stacked mass profile of the CLASH X-ray-selected subsample

Model	M_{200c} ($10^{14} M_{\odot} h_{70}^{-1}$)	c_{200c}	Shape/structural parameters	b_h	χ^2/dof	PTE ^a	Notes
NFW	$14.4^{+1.1}_{-1.0}$	$3.76^{+0.29}_{-0.27}$	$\gamma_c = 1$	—	11.3/11	0.419	No truncation
gNFW	$14.1^{+1.1}_{-1.1}$	$4.04^{+0.53}_{-0.52}$	$\gamma_c = 0.85^{+0.22}_{-0.31}$	—	10.9/10	0.366	No truncation
Einasto	$14.7^{+1.1}_{-1.1}$	$3.53^{+0.36}_{-0.39}$	$\alpha_E = 0.232^{+0.042}_{-0.038}$	—	11.7/10	0.306	No truncation
DARKexp- γ^b	$14.5^{+1.2}_{-1.1}$	$3.53^{+0.42}_{-0.42}$	$\phi_0 = 3.90^{+0.41}_{-0.45}$	—	13.5/10	0.198	No truncation
Pseudo isothermal	—	—	$V_c = 1762^{+40}_{-39}$ km/s, $r_c = 69^{+7}_{-7}$ kpc	—	23.6/11	0.015	No truncation
Burkert	$11.6^{+0.8}_{-0.8}$	—	$r_{200c}/r_0 = 8.81^{+0.42}_{-0.41}$	—	29.9/11	0.002	No truncation
Power-law sphere	$12.5^{+0.8}_{-0.8}$	—	$\gamma_c = 1.78^{+0.02}_{-0.02}$	—	93.5/11	0.000	No truncation
Halo model ^c :							
NFW+LSS (i)	$14.1^{+1.0}_{-1.0}$	$3.79^{+0.30}_{-0.28}$	$\gamma_c = 1$	9.3	10.9/11	0.450	Λ CDM $b_h(M)$ scaling
NFW+LSS (ii)	$14.4^{+1.4}_{-1.3}$	$3.74^{+0.33}_{-0.30}$	$\gamma_c = 1$	$7.4^{+4.6}_{-4.7}$	10.8/10	0.377	b_h as a free parameter
Einasto+LSS (i)	$14.3^{+1.1}_{-1.1}$	$3.69^{+0.36}_{-0.42}$	$\alpha_E = 0.248^{+0.051}_{-0.047}$	9.3	10.7/10	0.385	Λ CDM $b_h(M)$ scaling
Einasto+LSS (ii)	$14.5^{+1.9}_{-1.6}$	$3.65^{+0.47}_{-0.61}$	$\alpha_E = 0.245^{+0.061}_{-0.053}$	$8.7^{+5.3}_{-5.6}$	10.6/9	0.301	b_h as a free parameter
DARKexp+LSS (i)	$14.2^{+1.2}_{-1.1}$	$3.64^{+0.44}_{-0.46}$	$\phi_0 = 3.89^{+0.51}_{-0.54}$	9.3	11.7/10	0.308	Λ CDM $b_h(M)$ scaling
DARKexp+LSS (ii)	$14.0^{+1.8}_{-1.6}$	$3.69^{+0.53}_{-0.57}$	$\phi_0 = 3.85^{+0.57}_{-0.61}$	$10.1^{+4.9}_{-5.1}$	11.6/9	0.235	b_h as a free parameter

^a Probability to exceed the observed χ^2 value.

^b We use Dehnen–Tremaine γ -models with the central cusp slope $\gamma_c = 3 \log_{10} \phi_0 - 0.65$ ($1.7 \leq \phi_0 \leq 6$) as an analytic fitting function for the DARKexp density profile.

^c For halo model predictions, we decompose the total mass overdensity $\Delta\rho(r) = \rho(r) - \bar{\rho}_m$ as $\Delta\rho = f_t \rho_h + \rho_{2h}$ where $\rho_h(r)$ is the halo density profile, $\rho_{2h}(r) = \bar{\rho}_m b_h \xi_m^L(r)$ is the two-halo term, and $f_t(r) = (1 + r^2/r_t^2)^{-2}$ describes the steepening of the density profile in the transition regime around the truncation radius r_t , which is assumed to be $r_t = 3r_{200c}$.

- Consistent with cuspy density profiles (NFW, Einasto, DARKexp)
- Cuspy models that include Λ CDM 2-halo term ($b_h \sim 9.3$) give improved fits
- The best model reproduces the observed Einstein radius, $R_{\text{Ein}} \sim 20''$ at $z_s=2$



Concentration—Mass Relation of the CLASH X-ray-selected Subsample

Umetsu et al. 2015b, arXiv:1507.04385



Concentration—Mass Scaling Relation

Consider a power-law scaling relation of the form:

$$c_{200c} = 10^\alpha \left(\frac{M_{200c}}{M_{\text{piv}}} \right)^\beta \left(\frac{1+z}{1+z_{\text{piv}}} \right)^\gamma,$$

with pivot mass and redshift $M_{\text{piv}} = 10^{15} M_{\text{sun}} / h$, $z_{\text{piv}} = 0.34$

Define new independent (X) and dependent (Y) variables:

$$Y \equiv \log_{10} \left[\left(\frac{1+z}{1+z_{\text{piv}}} \right)^{-\gamma} c_{200c} \right], \quad Y = \alpha + \beta X$$

$$X \equiv \log_{10} (M_{200c} / M_{\text{piv}}).$$

Redshift slope γ is fixed to the theoretical prediction for the CLASH sample, $\gamma = -0.668$ (Meneghetti+14)



Bayesian Regression Analysis

We take into account

- Covariance between observed M and c
- Intrinsic scatter in c
- Non-uniformity in mass probability distribution $P(\log M)$

Conditional probability $P(y|x)$ with $(x,y) = \text{observed } (X,Y)$

$$\ln \mathcal{P}(\mathbf{y}|\mathbf{x}) = -\frac{1}{2} \sum_n \left[\ln (2\pi\sigma_n^2) + \left(\frac{y_n - \langle y_n|x_n \rangle}{\sigma_n} \right)^2 \right], \quad (35)$$

where $\langle y_n|x_n \rangle$ and $\sigma_n^2 \equiv \text{Var}(y_n|x_n)$ are the conditional mean and variance of y_n given x_n , respectively:

$$\begin{aligned} \langle y_n|x_n \rangle &= \alpha + \beta\mu + \frac{\beta\tau^2 + C_{xy,n}}{\tau^2 + C_{xx,n}}(x_n - \mu), \\ \sigma_n^2 &= \beta^2\tau^2 + \sigma_{Y|X}^2 + C_{yy,n} - \frac{(\beta\tau^2 + C_{xy,n})^2}{\tau^2 + C_{xx,n}}, \end{aligned} \quad (36)$$

where $\sigma_{Y|X}$ is the intrinsic scatter in the $Y-X$ relation;



Marginalized Posterior Distributions

$$c_{200c} = 10^\alpha \left(\frac{M_{200c}}{M_{\text{piv}}} \right)^\beta \left(\frac{1+z}{1+z_{\text{piv}}} \right)^\gamma$$

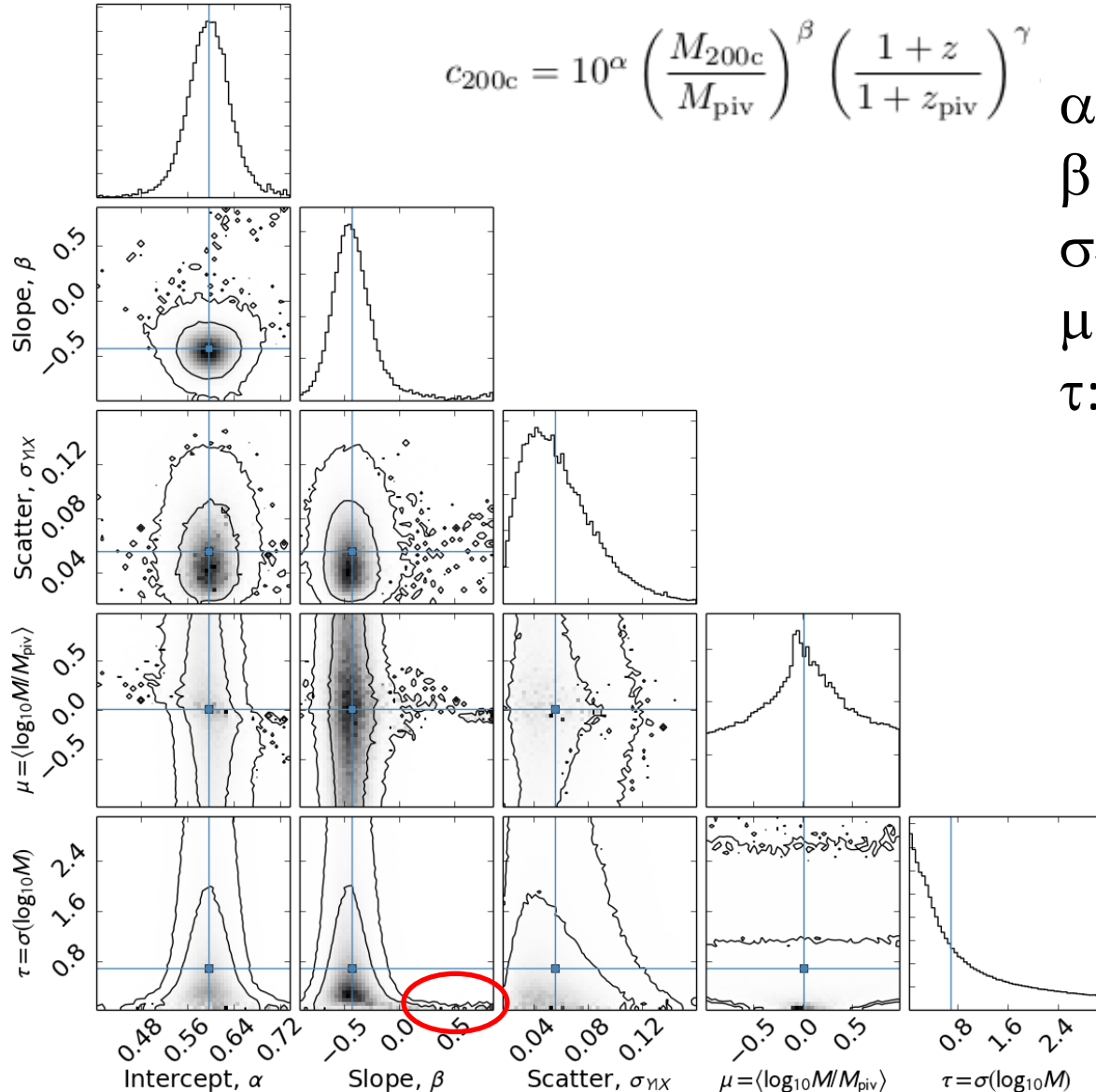
α : intercept

β : slope

$\sigma_{Y|X}$: scatter

μ : Gaussian mean of $P(\ln M)$

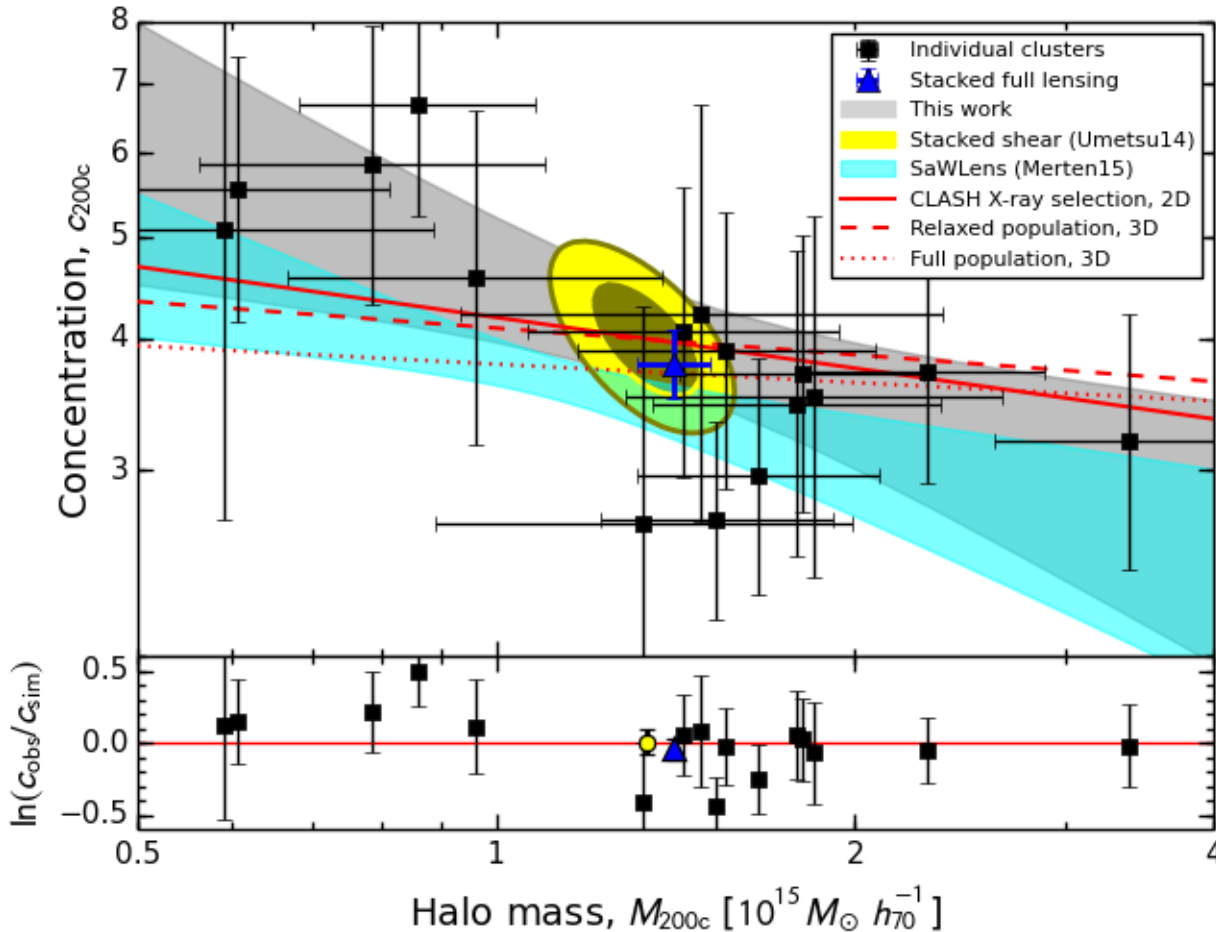
τ : Gaussian width of $P(\ln M)$



High β tail associated with small τ : i.e., localized $P(\ln M)$



CLASH: Lensing Observations vs. Predictions



$$c_{200c} \Big|_{z=0.34} = 3.95 \pm 0.35$$

$$\text{at } M_{200c} = 10^{15} M_{\text{sun}} / h,$$

$$\sigma(\ln c_{200c}) = 0.13 \pm 0.06$$

Normalization, slope, & scatter are all consistent with LCDM when the CLASH selection function based on X-ray morphological regularity and the projection effects are taken into account



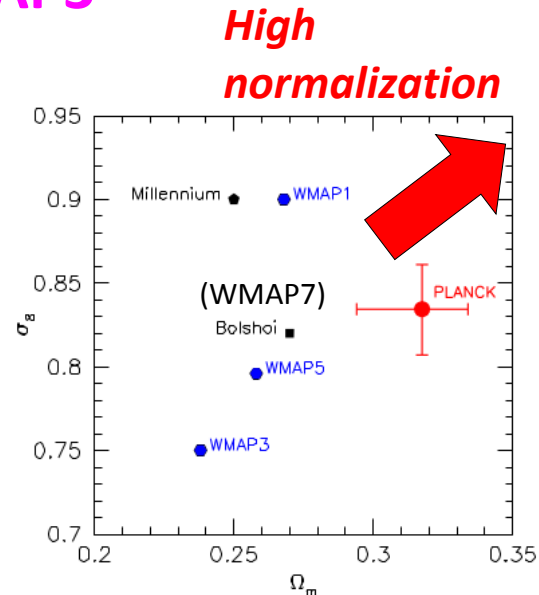
Comparison with LCDM Models

Table 5

Comparison of measured and predicted concentrations for the CLASH X-ray-selected subsample

Author	Sample	3D/2D	Function ^a	$c^{(obs)}/c^{(pred)}$ Average ^c	σ^d	χ^2	PTE ^b
Theory:							
Duffy et al. (2008)	full	3D	$c-M$	1.331 ± 0.108	0.334	22.6	0.046
Duffy et al. (2008)	relaxed	3D	$c-M$	1.165 ± 0.094	0.290	13.6	0.399
Prada et al. (2012)	full	3D	$c-\nu$	0.733 ± 0.065	0.244	24.6	0.026
Bhattacharya et al. (2013)	full	3D	$c-\nu$	1.169 ± 0.095	0.292	14.1	0.369
Bhattacharya et al. (2013)	relaxed	3D	$c-\nu$	1.131 ± 0.092	0.277	12.4	0.494
Dutton & Macciò (2014)	full	3D	$c-M$	1.061 ± 0.086	0.262	10.4	0.659
Meneghetti et al. (2014)	full	3D	$c-M$	1.061 ± 0.089	0.279	10.2	0.675
Meneghetti et al. (2014)	relaxed	3D	$c-M$	0.990 ± 0.083	0.249	9.2	0.760
Diemer & Kravtsov (2015)	full (median)	3D	$c-\nu$	1.021 ± 0.083	0.330	14.4	0.349
Diemer & Kravtsov (2015)	full (mean)	3D	$c-\nu$	1.060 ± 0.086	0.326	13.8	0.391
Meneghetti et al. (2014)	full	2D	$c-M$	1.087 ± 0.092	0.336	13.5	0.413
Meneghetti et al. (2014)	relaxed	2D	$c-M$	1.040 ± 0.086	0.283	10.8	0.628
Meneghetti et al. (2014)	CLASH	2D	$c-M$	0.988 ± 0.078	0.227	9.6	0.730
Observations:							
Merten et al. (2015)	CLASH	2D	$c-M$	1.133 ± 0.087	0.209	9.2	0.754

WMAP3



^a $c-M$: power-law $c(M, z)$ relation; $c-\nu$: halo concentration given as a function of peak height $\nu(M, z)$.

^b Probability to exceed the measured χ^2 value assuming the standard χ^2 probability distribution function.

^c Weighted geometric average of observed-to-predicted concentration ratios.

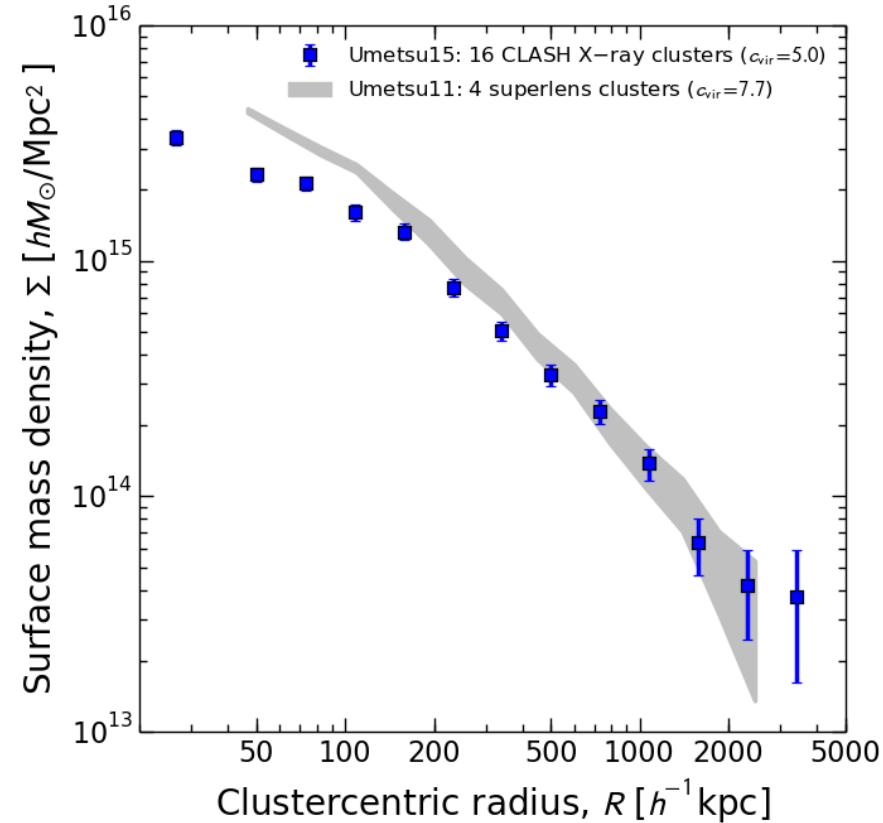
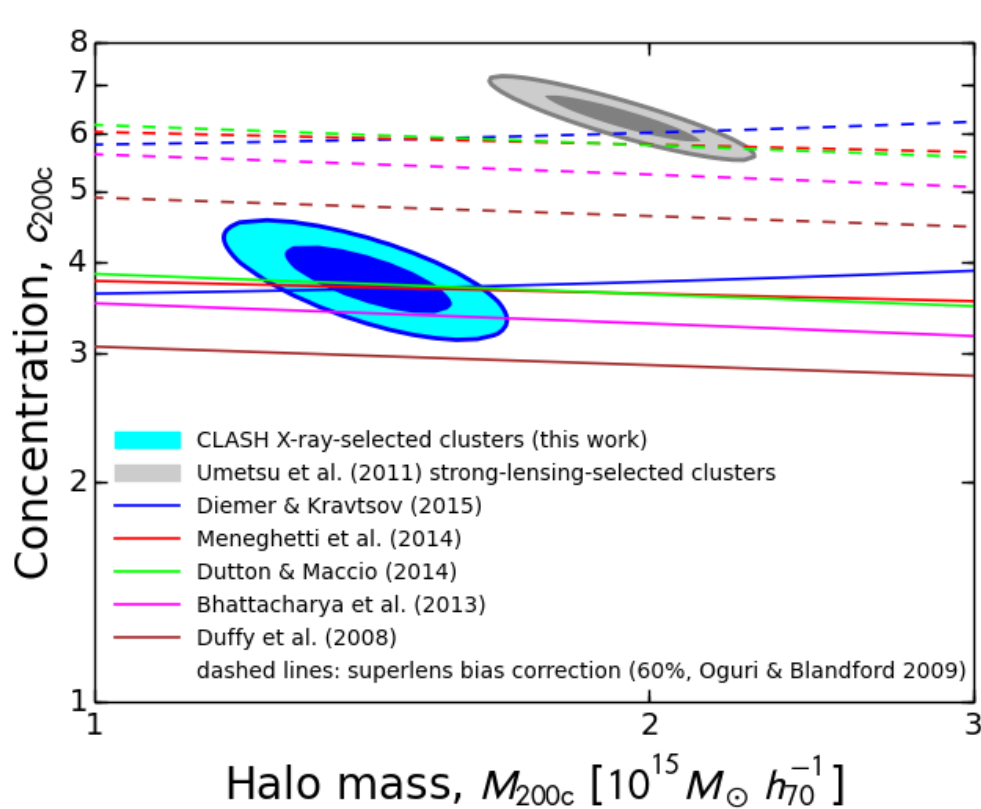
^d Standard deviation of the distribution of observed-to-predicted concentration ratios.

- Consistent with models that are calibrated for more recent cosmologies (WMAP7 and later)
- Better agreement is achieved when selection effects (overall degree of relaxation) are taken into account



X-ray Regular vs. Superlens Clusters

Umetsu+11b: 4 *superlens* clusters with $R_{\text{Ein}} > 30''$ at $z_s=2$ (A1689, A1703, Cl0024, A370)



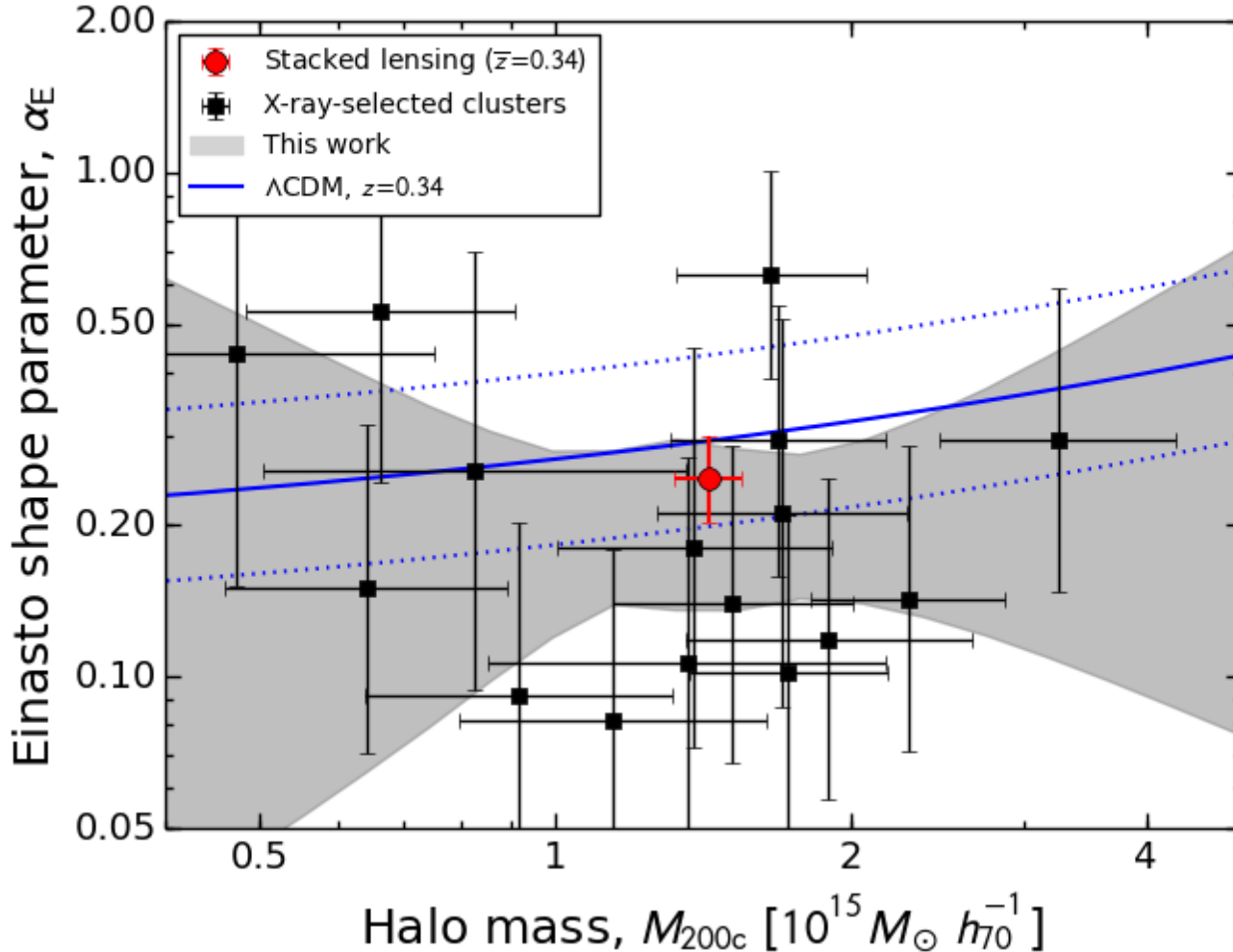
Higher normalization LCDM cosmology (WMAP7 and later) + “predicted” +60% superlens correction (e.g., Oguri+Blandford09) can explain superlens mass profiles!



Einasto Shape Parameter vs. Halo Mass

α_E : degree of curvature of the Einasto density profile

$$\frac{d \ln \rho(r)}{d \ln r} = -2 \left(\frac{r}{r_{-2}} \right)^{\alpha_E}$$



$$\alpha_E \approx 0.155 + 0.0095v^2 \text{ (Gao + 08)}$$

$$v = \frac{\delta_c}{\sigma(M)}$$

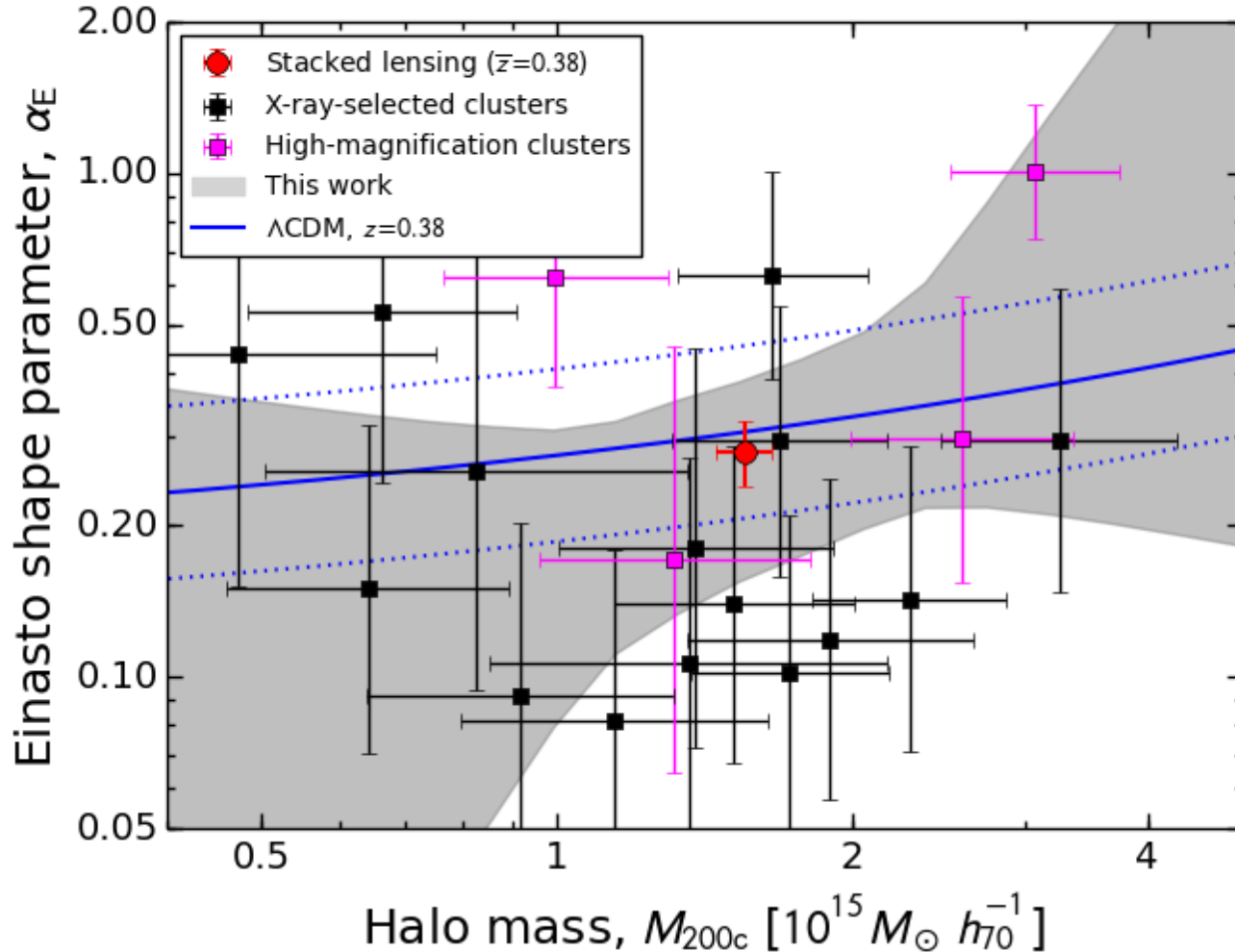
Preliminary results



Einasto Shape Parameter vs. Halo Mass

α_E : degree of curvature of the Einasto density profile

$$\frac{d \ln \rho(r)}{d \ln r} = -2 \left(\frac{r}{r_{-2}} \right)^{\alpha_E}$$



$$\alpha_E \approx 0.155 + 0.0095v^2 \quad (\text{Gao} + 08)$$

$$v = \frac{\delta_c}{\sigma(M)}$$

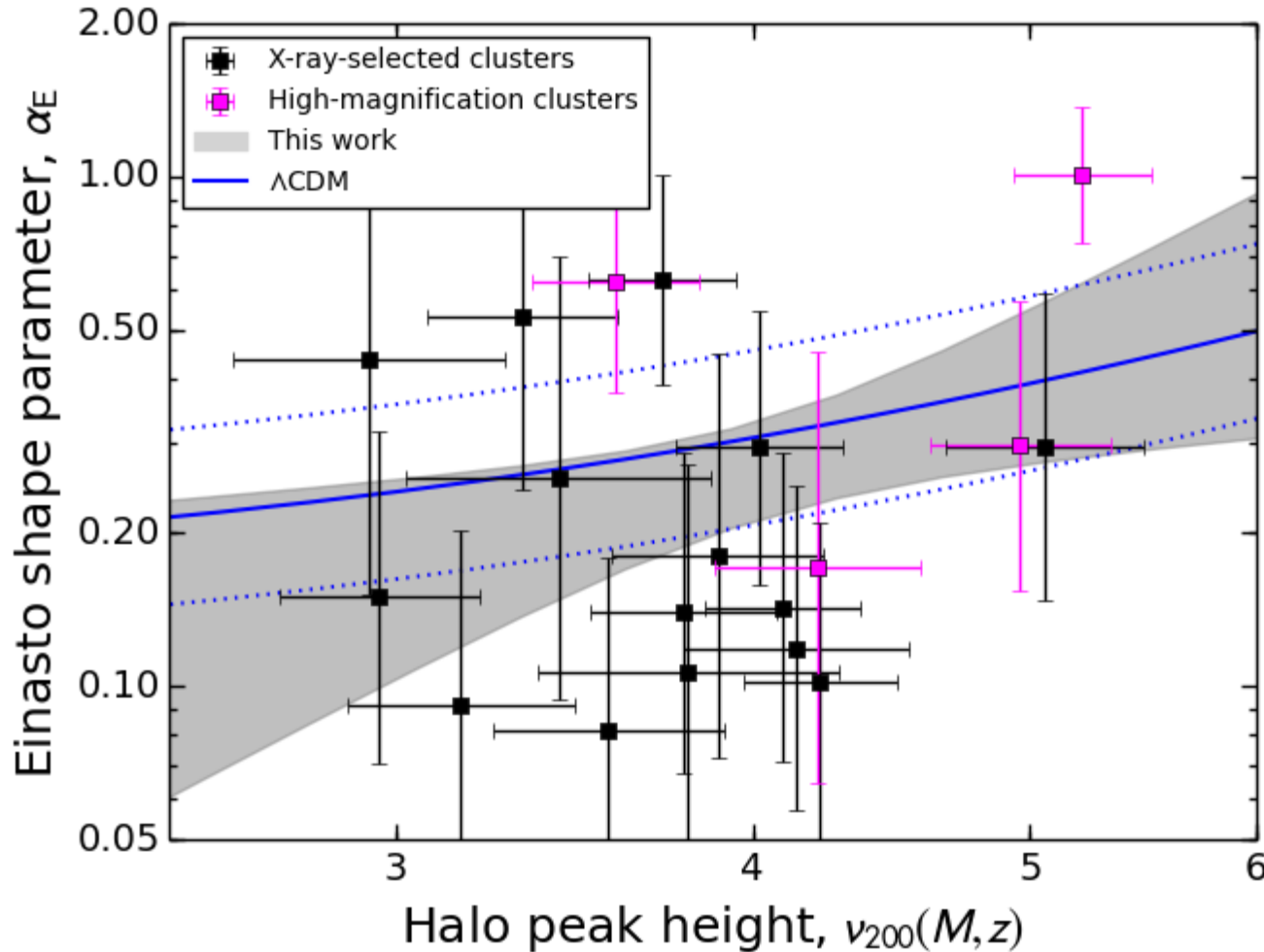
Preliminary results



Einasto Shape Parameter vs. Halo Peak Height

α_E : degree of curvature of the Einasto density profile

$$\frac{d \ln \rho(r)}{d \ln r} = -2 \left(\frac{r}{r_{-2}} \right)^{\alpha_E}$$



$$\alpha_E \approx 0.155 + 0.0095v^2 \text{ (Gao + 08)}$$

$$v = \frac{\delta_c}{\sigma(M)}$$

**Preliminary
results**



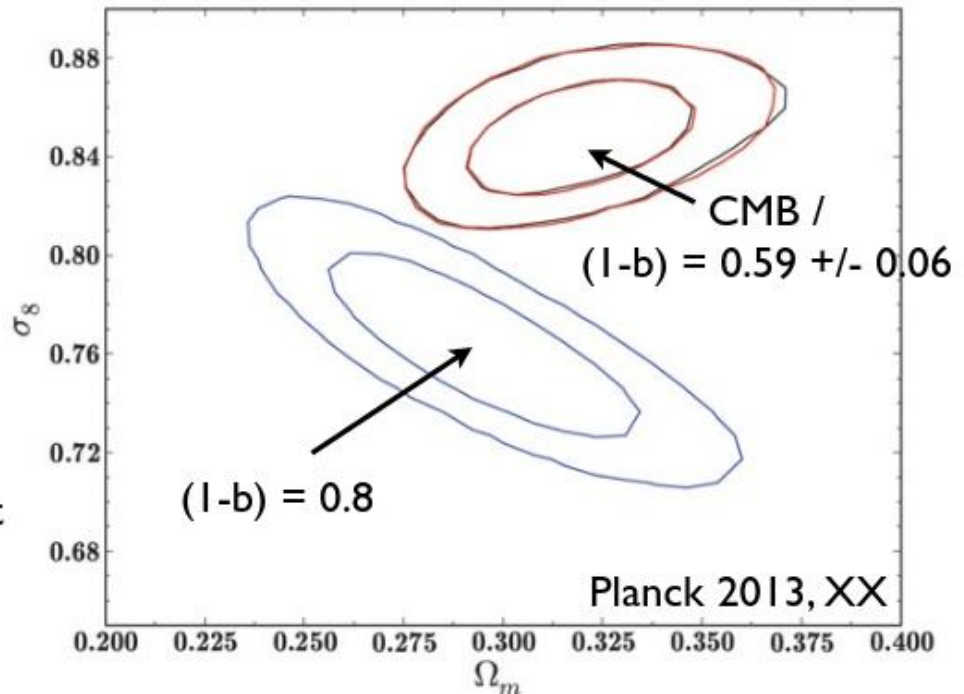
Ensemble Calibration of Cluster Masses

Umetsu et al. 2015b, arXiv:1507.04385

Planck13 CMB vs. Cluster Cosmology

$b=0.2?? - 0.4??$

- Planck: 3σ tension between SZ cluster counts and CMB cosmology
- assumes $M_{\text{Planck}} / M_{\text{true}} = (1-b) = 0.8$
- calibrated with XMM hydrostatic masses (Arnaud et al. 2010) + simulations



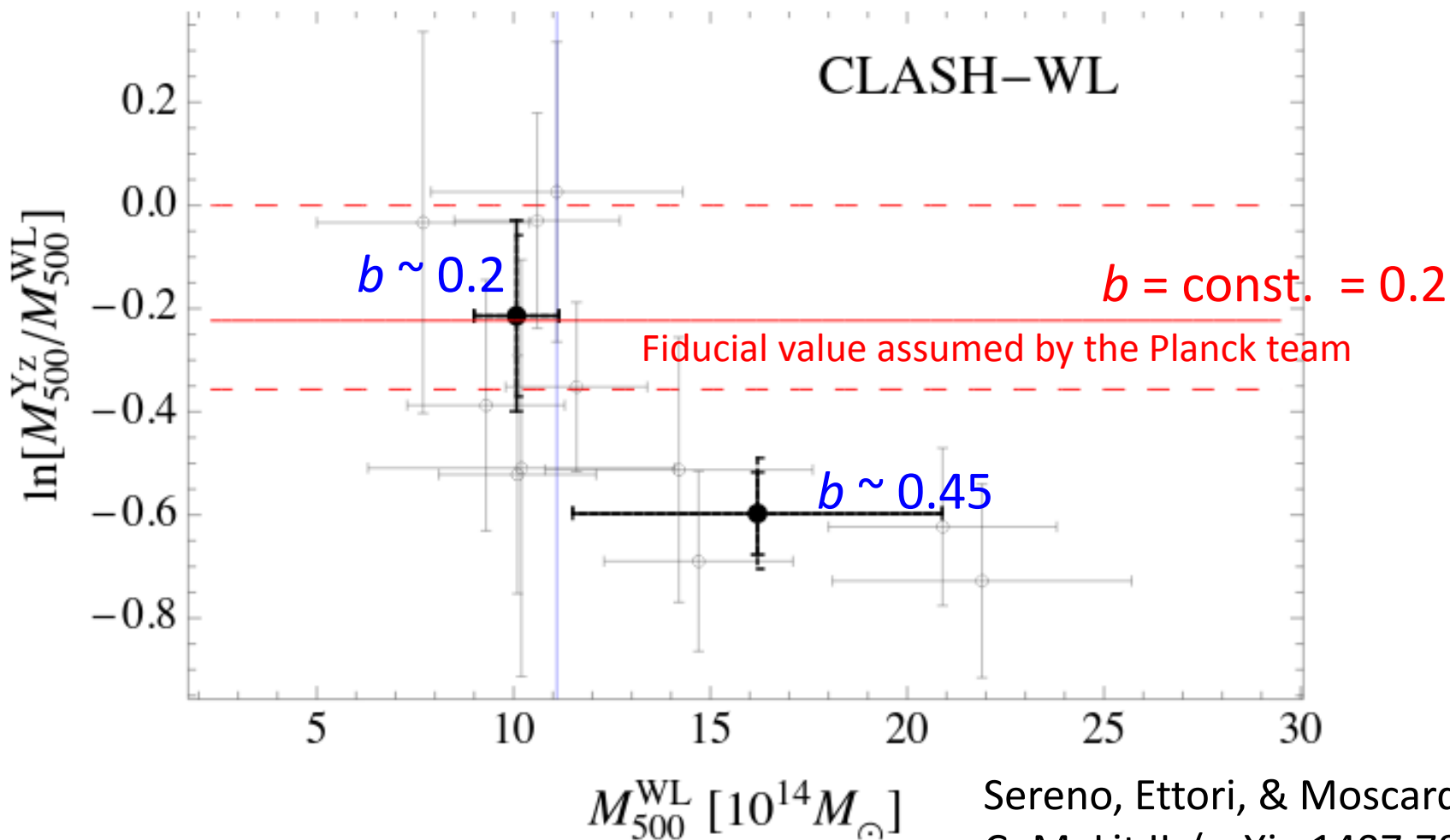
suggested explanations:

- **mass bias underestimated** (and no accounting for uncertainties)
- 2.9σ detection of neutrino masses: $\Sigma m_\nu = (0.58 \pm 0.20) \text{ eV}$
(Planck+WMAPpol+ACT+BAO: $\Sigma m_\nu < 0.23 \text{ eV}$, 95% CL)

Slide taken from Anja von der Linden's presentation

Comparison with *Planck* Masses: *It's not so simple!!!*

Mass-dependent bias (20-45%) observed for *Planck* mass estimates

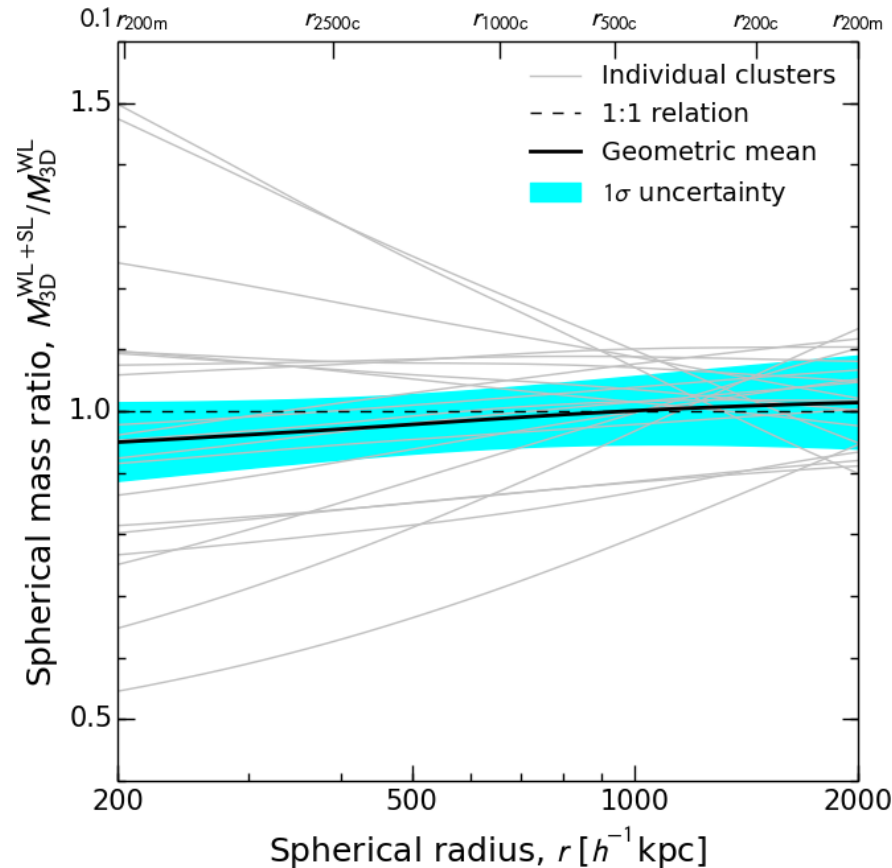




CLASH Internal Consistency

$M(<r)$ de-projected assuming spherical NFW density profiles

$$\left\langle \frac{M_{3D}(\text{WL} + \text{SL})}{M_{3D}(\text{WL})} \right\rangle$$



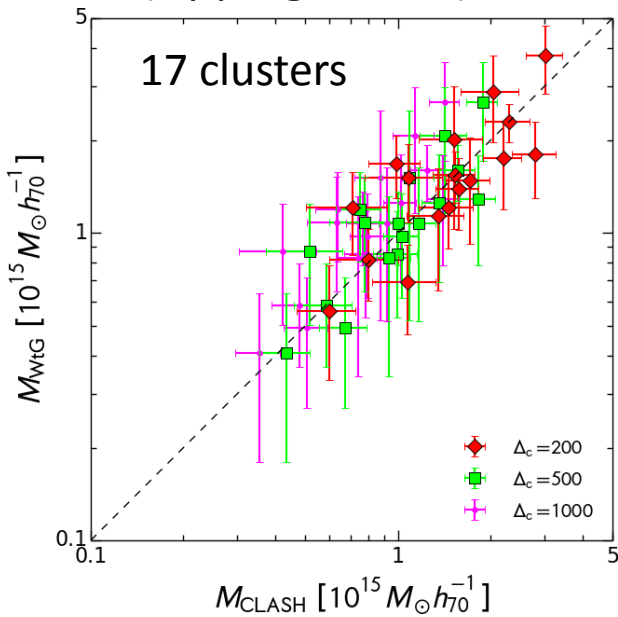
Umetsu+15b,
arXiv:1507.04385

Systematic uncertainty in the overall mass calibration is empirically derived to be $< 5\%$, which is insignificant compared to the statistical uncertainty of $\sim 6\%$ with $N=20$ clusters



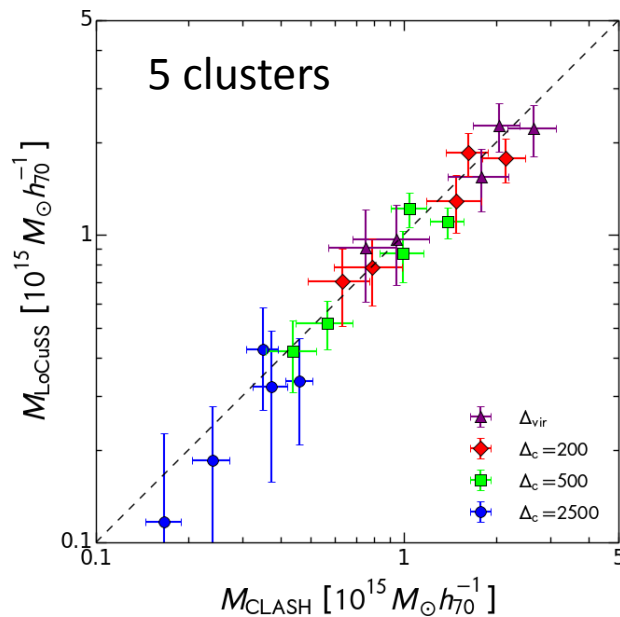
Mass Comparisons with Other WL Surveys

WtG [Subaru]
(Applegate+14)



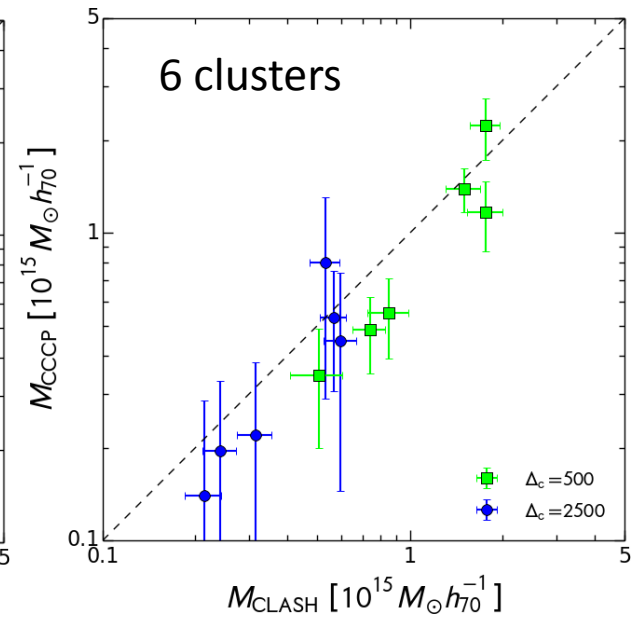
$$\begin{aligned} \langle M_{\text{WtG}} / M_{\text{CLASH}} \rangle &= 1.03 \pm 0.09 \quad (\Delta = 200) \\ &= 1.07 \pm 1.12 \quad (\Delta = 500) \\ &= 1.07 \pm 1.12 \quad (\Delta = 1000) \end{aligned}$$

LoCuSS [Subaru]
(Okabe & Smith 15)



$$\begin{aligned} \langle M_{\text{LoCuSS}} / M_{\text{CLASH}} \rangle &= 1.00 \pm 0.15 \quad (\Delta = \Delta_{\text{vir}}) \\ &= 0.98 \pm 0.13 \quad (\Delta = 200) \\ &= 0.93 \pm 0.10 \quad (\Delta = 500) \\ &= 0.84 \pm 0.22 \quad (\Delta = 2500) \end{aligned}$$

CCCP [CFHT]
(Hoekstra+15)



$$\begin{aligned} \langle M_{\text{CCCP}} / M_{\text{CLASH}} \rangle &= 0.84 \pm 0.10 \quad (\Delta = 500) \\ &= 0.91 \pm 0.24 \quad (\Delta = 2500) \end{aligned}$$

Umetsu+15b,
arXiv:1507.04385



Summary

– Ensemble-averaged mass profile shape

- Data favor cuspy density profiles predicted for collisionless-DM-dominated halos in gravitational equilibrium (NFW, Einasto, DARKexp)
- The highest-ranked model is the 2-parameter NFW+LSS model including the 2-halo term using the LCDM b - M relation ($b_h \sim 9.3$)
- $c_{200c} = 3.8 \pm 0.3$ at $M_{200c} = 10^{15} M_{\text{sun}}/h$, $z=0.34$

– Concentration vs. mass relation

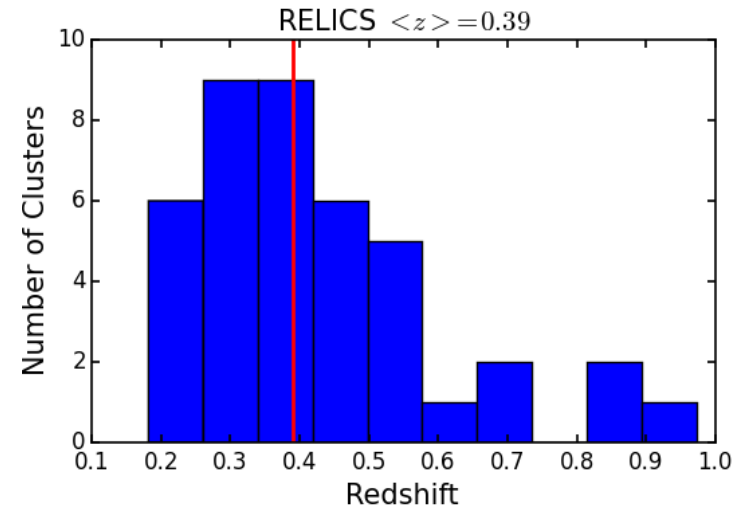
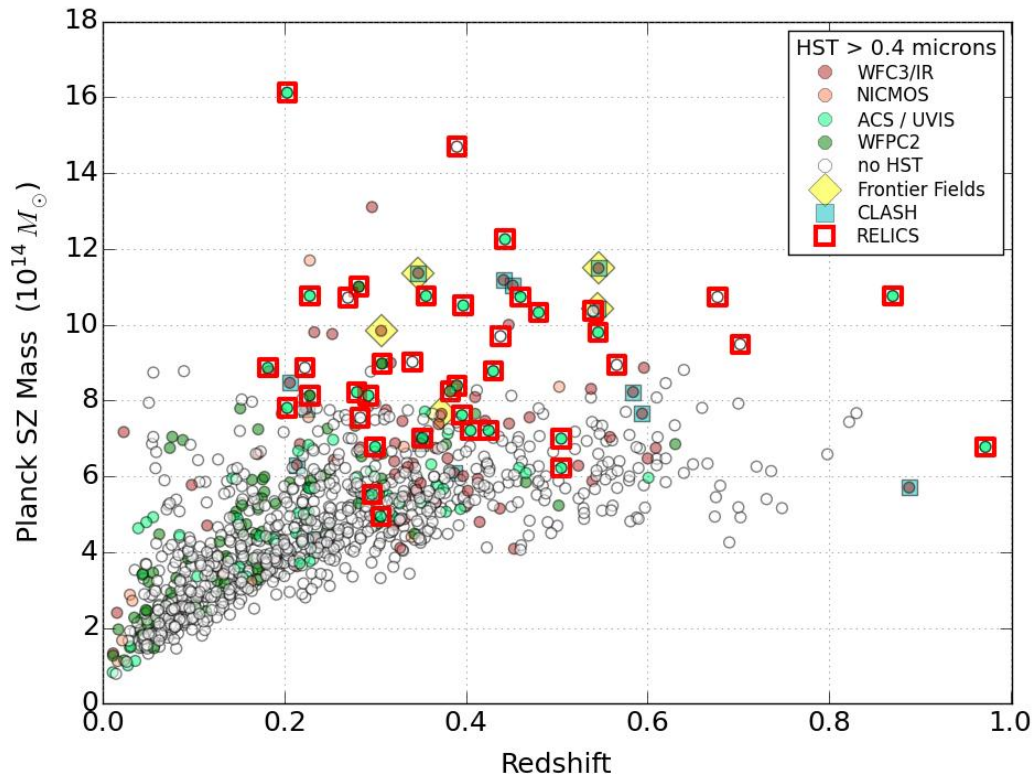
- Fully consistent with LCDM when the CLASH selection function based on X-ray morphological regularity and the projection effects are taken into account

– Mass calibration

- Internal consistency better than 5% \pm 6% by comparison with the WL-only analysis of Umetsu et al. (2014)

Reionization Lensing Cluster Survey (RELICS)

Newly approved 190-orbit *HST* survey (7 ACS/WFC3 filters) of 41 high-mass clusters primarily selected from the *Planck* survey (P.I. Dan Coe; Oct 2015 – Apr 2017)



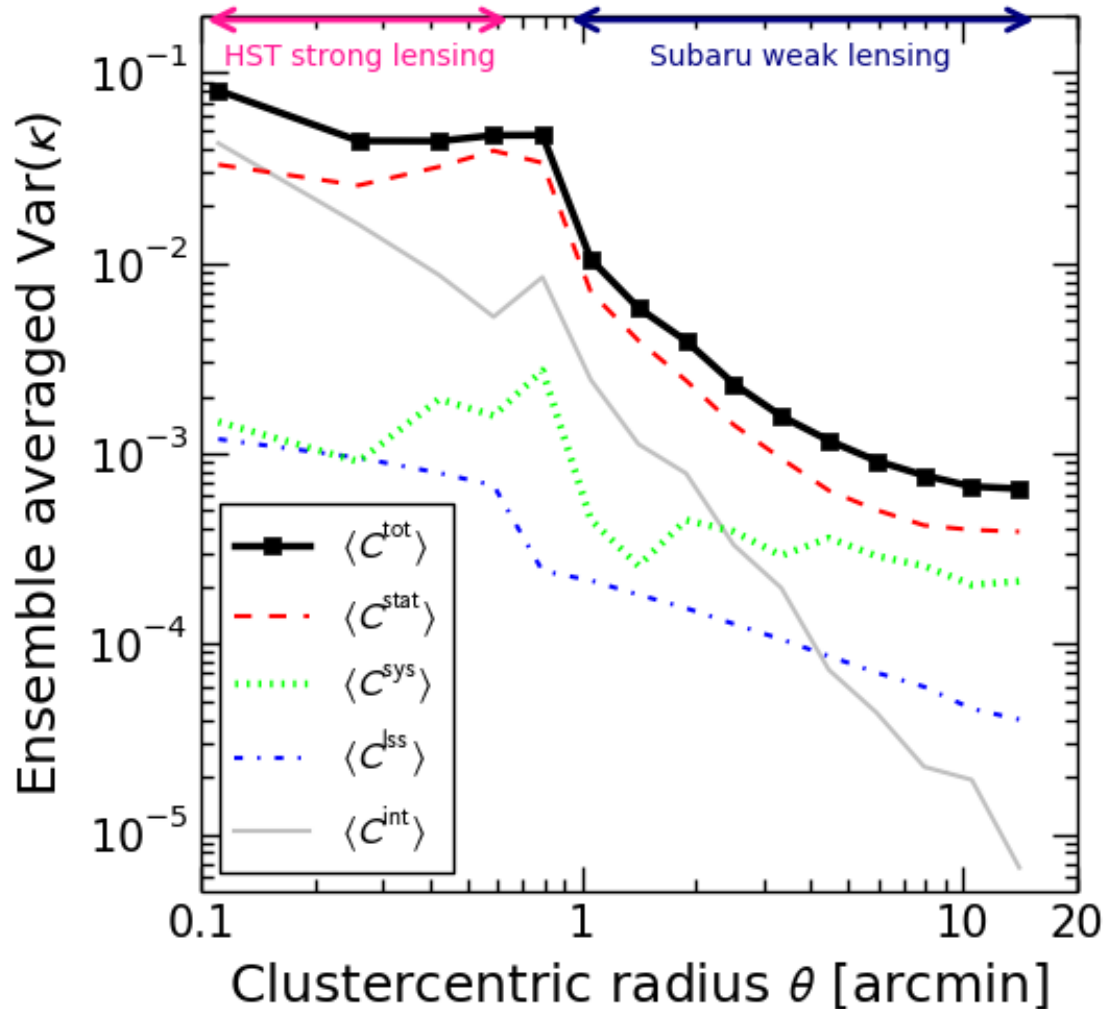
<http://hstrelics.weebly.com>

Supplemental Slides



Ensemble-averaged Error Budget

Diagonal elements (C_{ii}) averaged over all CLASH clusters



Residual mass-sheet uncertainty (Umetsu+14)

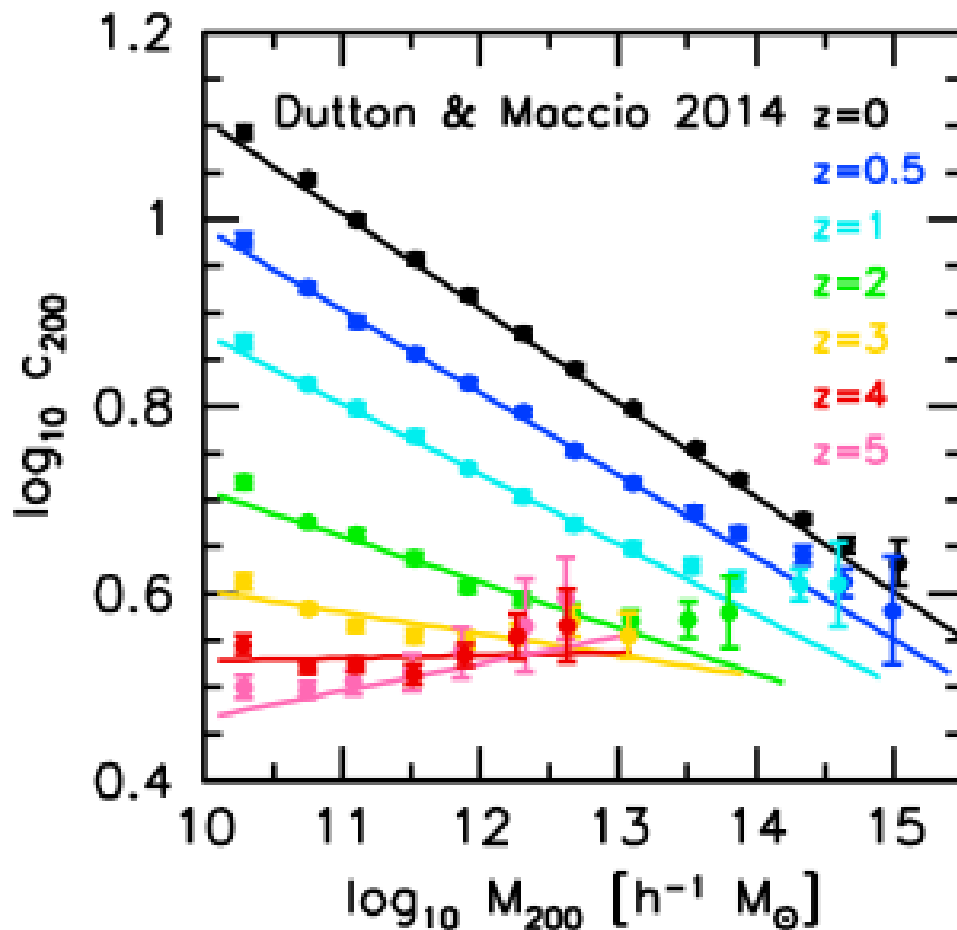
$$\langle C_{\text{sys}} \rangle_{ii} \sim \text{const.} \sim (0.02)^2$$

Intrinsic profile variations due to triaxiality, substructure, and c - M scatter (Gruen+15)

$$\langle C_{\text{int}} \rangle_{ii} \approx (0.2)^2 K_i^2$$

Degree of Mass Concentration

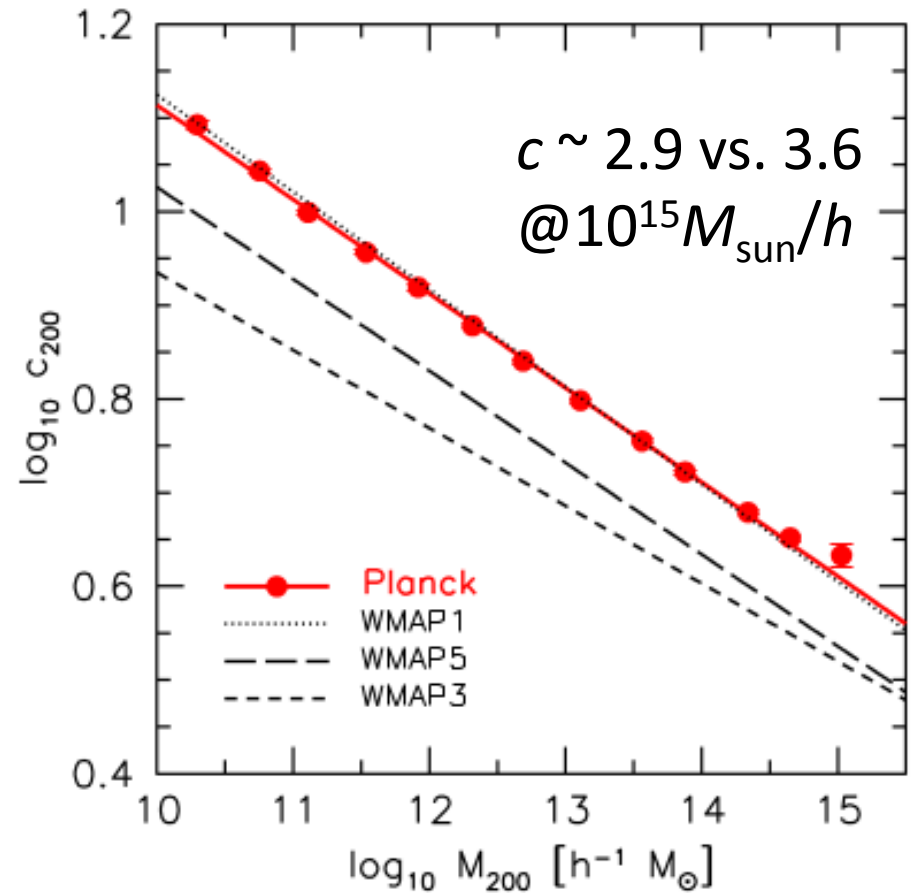
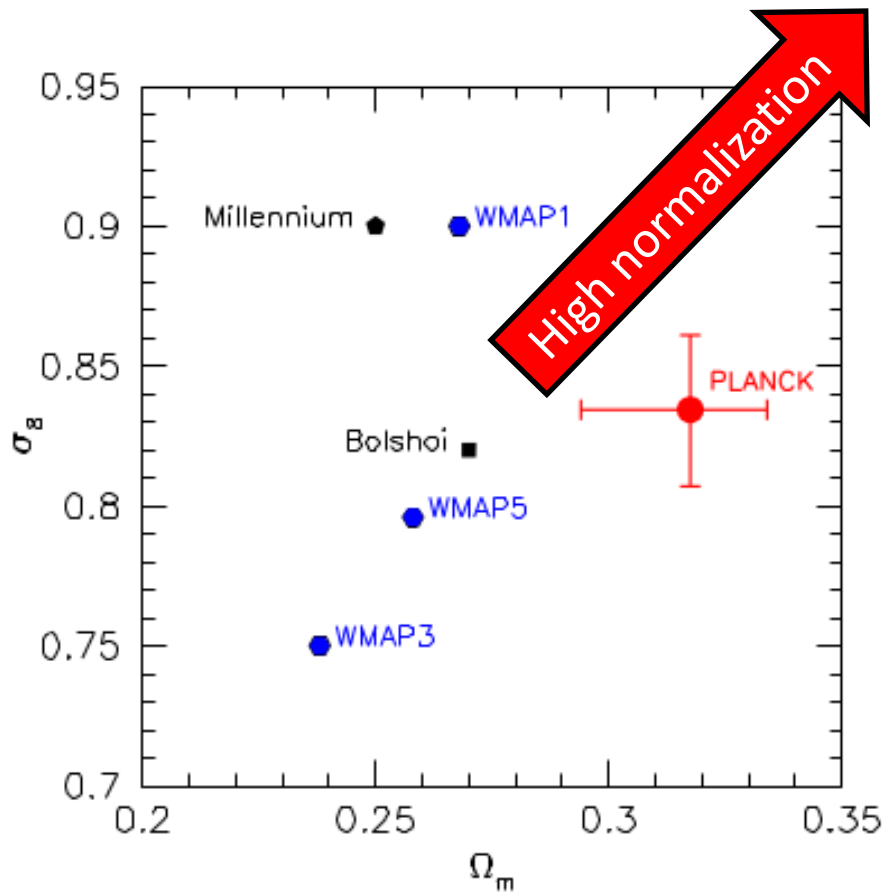
$$c_{200} \equiv \frac{r_{200}}{r_s} = \frac{\text{(Outer scale radius)}}{\text{(Inner scale radius)}}$$



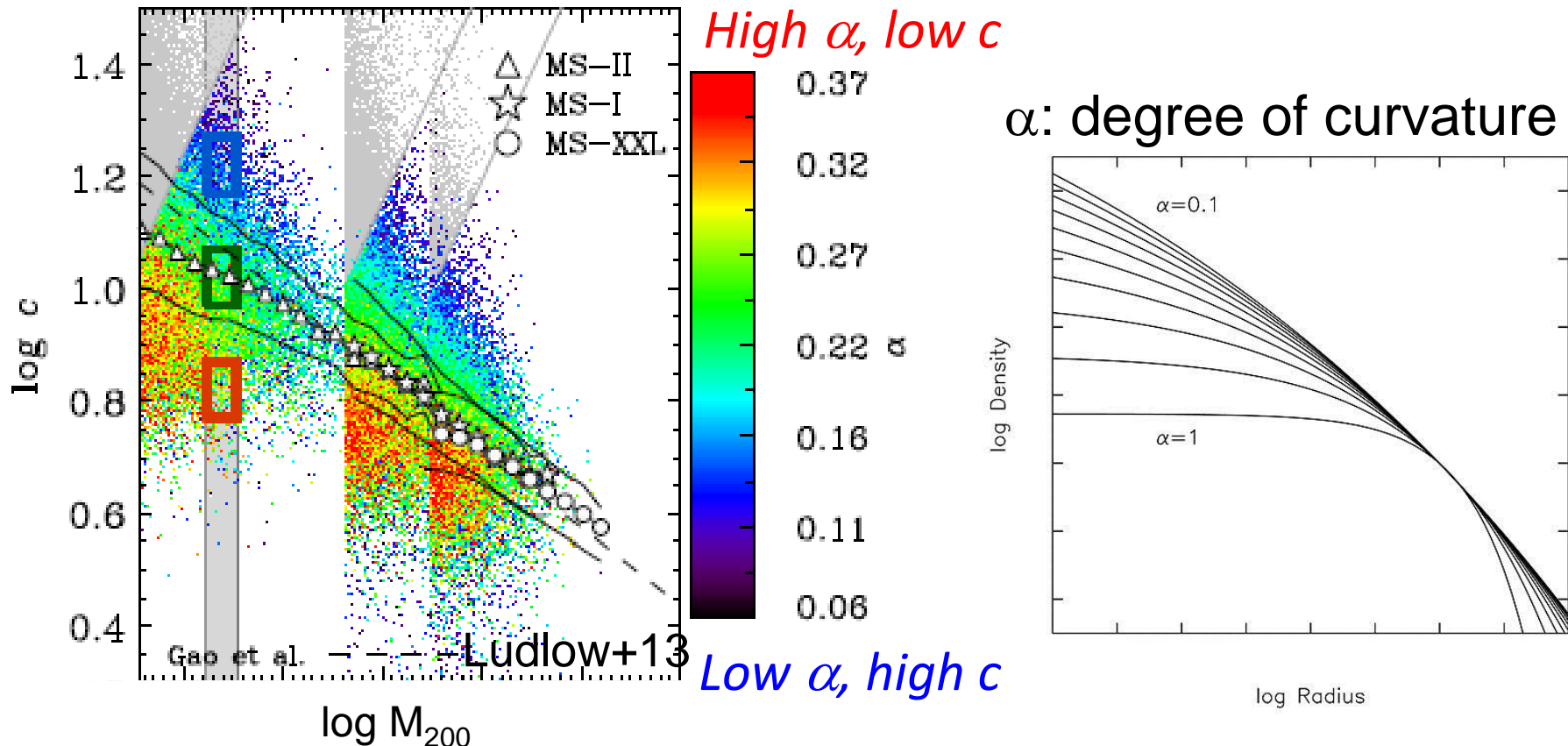
In hierarchical structure formation, $\langle c \rangle$ is predicted to correlate with M

DM halos that are more massive collapse later on average, when the mean background density of the universe is correspondingly lower (e.g., Bullock+01)

Concentration is sensitive to cosmology



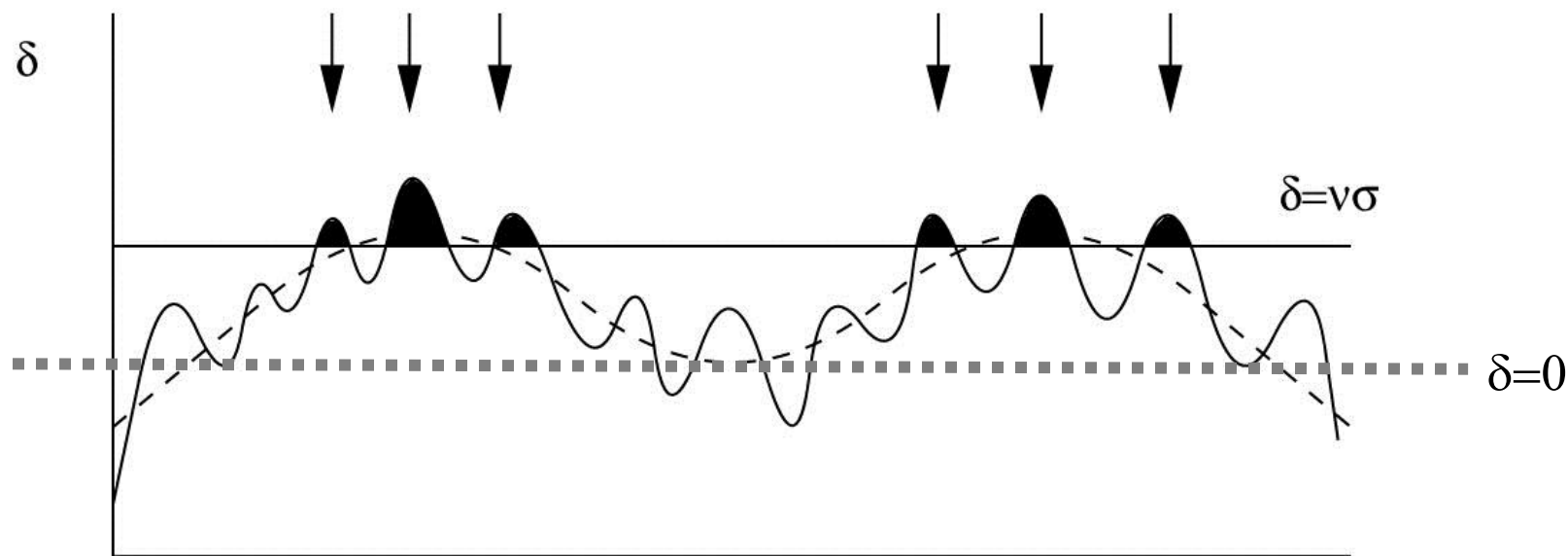
Intrinsic Scatter in $c(M)$: Mass Assembly Histories (MAH)



- Scatter is due to another DoF (α), related to MAH (Ludlow+13)
- Larger values of α correspond to halos that have been assembled more rapidly than the NFW curve
- Halos with average c_{200} have the NFW-equivalent $\alpha \sim 0.18$

Key Predictions of nonlinear structure formation models

(3) Halo bias: surrounding large-scale structure



$$\delta(\mathbf{x}) := \frac{\rho - \bar{\rho}}{\bar{\rho}} = \int \frac{d^3k}{(2\pi)^3} \tilde{\delta}(\mathbf{k}) e^{i\mathbf{k}\cdot\mathbf{x}} \quad \mathbf{x}$$

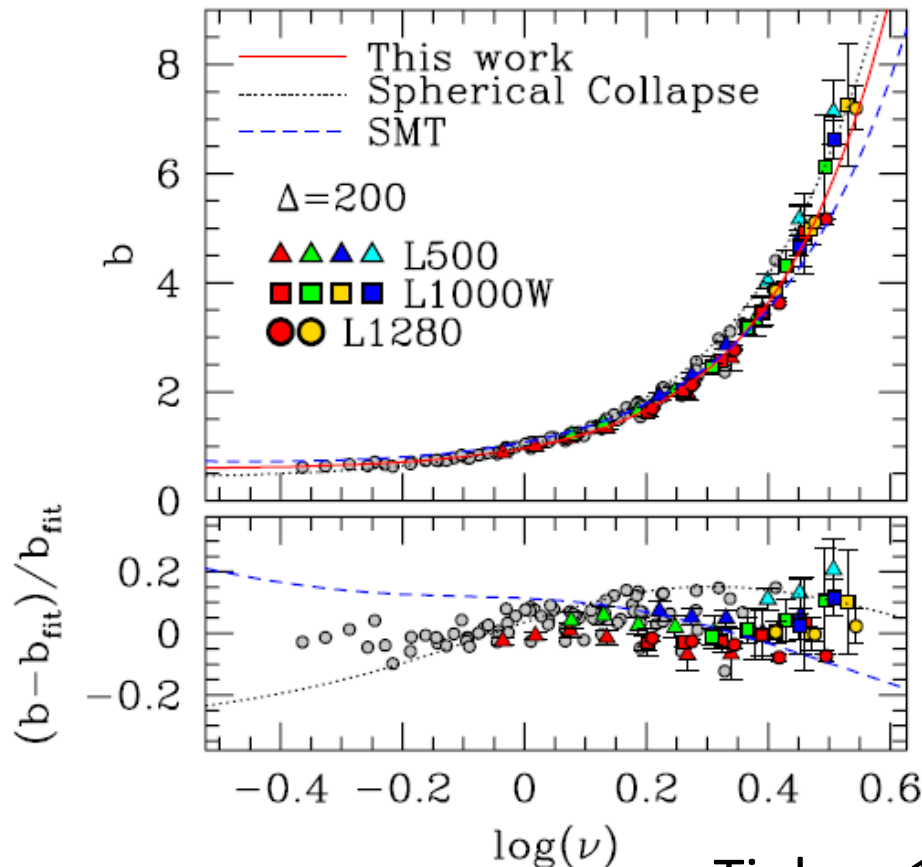
$$\langle \tilde{\delta}(\mathbf{k}) \tilde{\delta}(\mathbf{k}') \rangle = (2\pi)^3 \delta_D^3(\mathbf{k} + \mathbf{k}') P(k)$$

Halo Bias Factor: b_h

Clustering of matter
around halos with M :

$$\xi_{\text{hm}}(r | M) \equiv \langle \delta_h(\mathbf{x} | M) \delta_m(\mathbf{x} + \mathbf{r}) \rangle$$

$$= \frac{\langle \rho_h(r | M) \rangle}{\bar{\rho}} + \underline{b_h(M) \xi_{\text{mm}}(r)} \quad \text{2h term}$$



Correlated matter distribution (2h term)

Matter correlation function:

$$\xi_{\text{mm}}(\mathbf{r}) \equiv \langle \delta_m(\mathbf{x}) \delta_m(\mathbf{x} + \mathbf{r}) \rangle = \int \frac{d^3k}{(2\pi)^3} P(k) e^{i\mathbf{k} \cdot \mathbf{r}}$$

$$\propto \sigma_8^2$$

Linear halo bias:

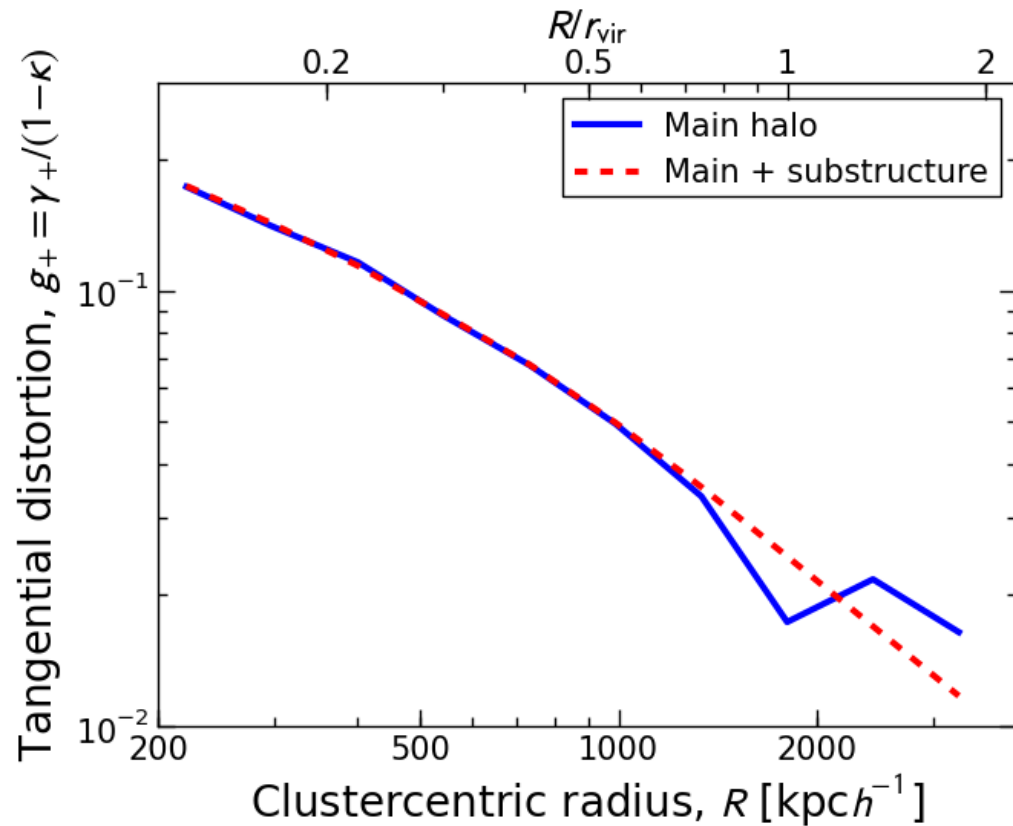
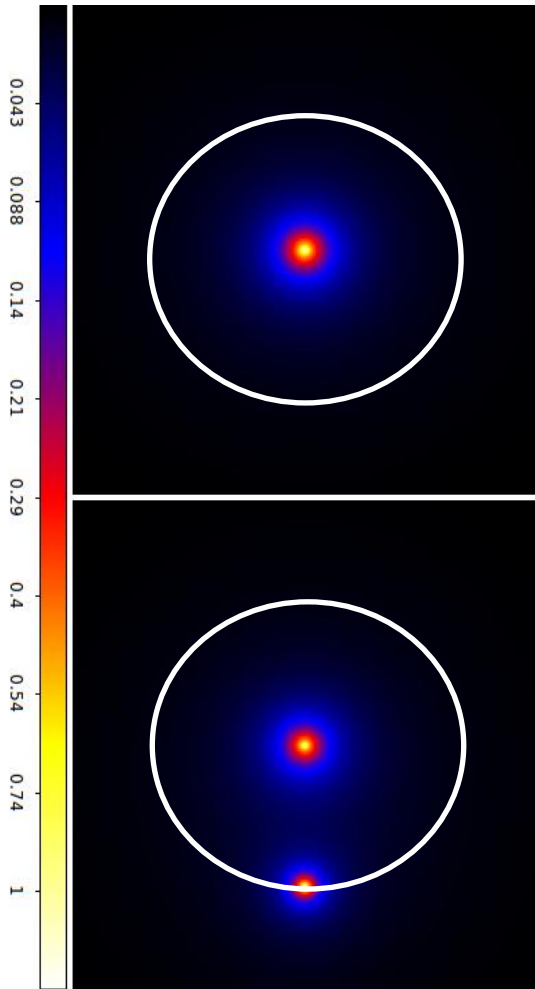
$$b_h(\nu) \approx 1 + \frac{\nu^2 - 1}{\delta_c}$$

$$\nu \equiv \frac{\delta_c}{\sigma(M, z)} \sim 3 - 4 \text{ for clusters}$$

Tinker+10 LCDM simulations

Non-local substructure effect

A substructure at $R \sim r_{\text{vir}}$ of the main halo, modulating $\Delta\Sigma(R) = \Sigma(< R) - \Sigma(R)$



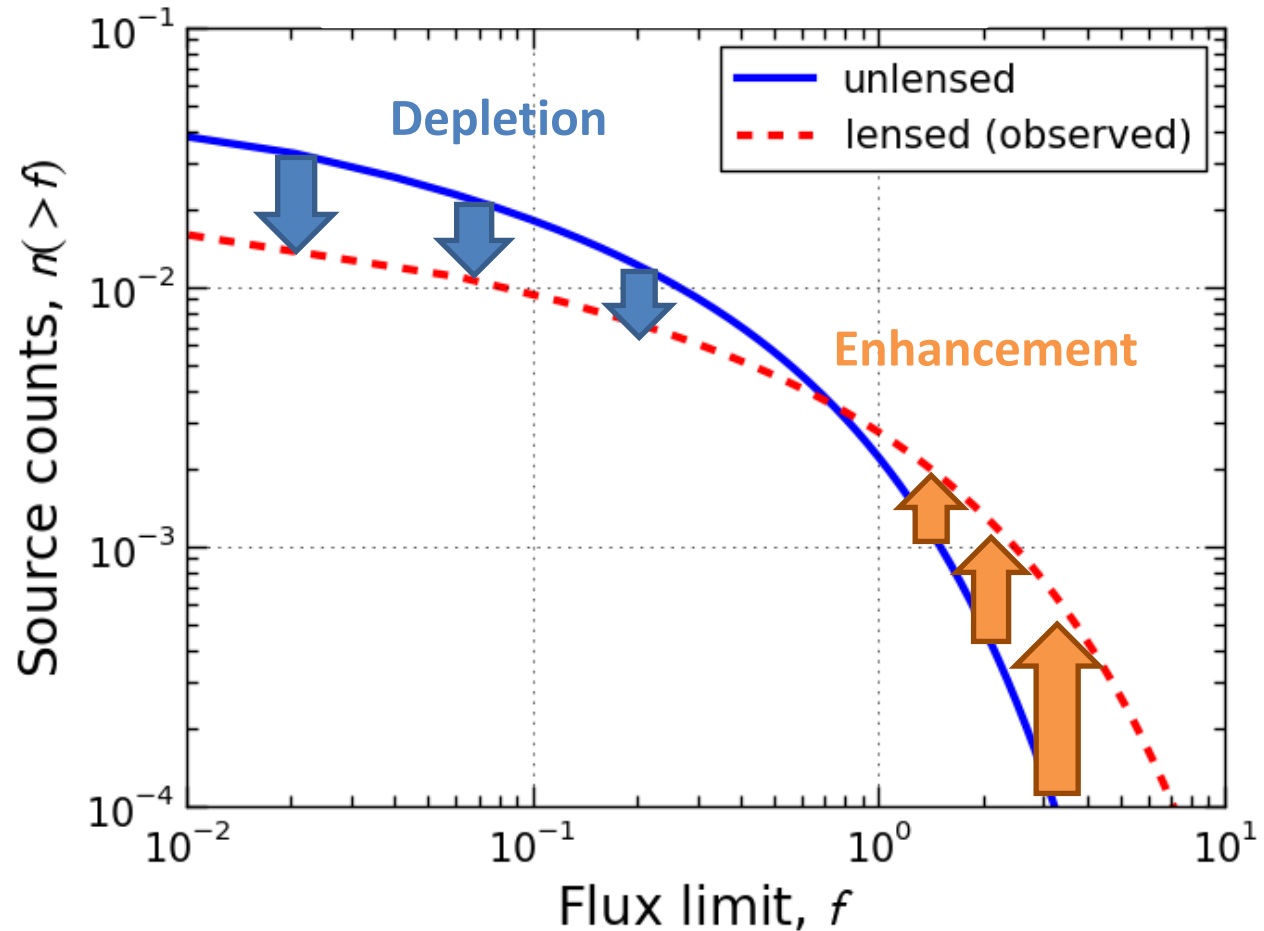
Known 5%-10% negative bias in mass estimates from tangential-shear fitting, inherent to rich substructure in outskirts (Rasia+12)

Magnification bias effects

Flux-limited
source counts:

$$n_{\text{obs}}(> f) = \mu^{-1} n(> \mu^{-1} f)$$

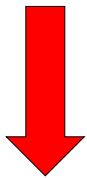
Broadhurst, Taylor &
Peacock 1995



Flux amplification



Geometric area
distortion



n/μ



Averaged Halo Density Profile $\Sigma(R)$

Stacking lensing signals of individual clusters by

$$\langle\langle \Sigma \rangle\rangle = \left(\sum_n \mathcal{W}_n \right)^{-1} \left(\sum_n \mathcal{W}_n \Sigma_n \right),$$

Summing over clusters ($n=1, 2, \dots$)

with individual “sensitivity” matrix

$$(\mathcal{W}_n)_{ij} \equiv \Sigma_{(c, \infty)n}^{-2} (C_n^{-1})_{ij},$$

defined with total covariance matrix

$$C = C^{\text{stat}} + C^{\text{sys}} + C^{\text{lss}} + C^{\text{int}},$$

With “trace-approximation”, averaging (stacking) is interpreted as

$$\langle\langle M_\Delta \rangle\rangle = \frac{\sum_n \text{tr}(\mathcal{W}_n) M_{\Delta,n}}{\sum_n \text{tr}(\mathcal{W}_n)}$$

Umetsu et al. 2014,
ApJ, 795, 163